NAVAL POSTGRADUATE SCHOOL

MONTEREY, CALIFORNIA

THESIS

A CLIMATOLOGICAL STUDY OF HURRICANE FORCE EXTRATROPICAL CYCLONES

by

Razaak Laiyemo

March 2012

Thesis Advisor: Richard Moore
Second Reader: Wendell Nuss

THIS PAGE INTENTIONALLY LEFT BLANK

REPORT DOCUMENTATION PAGE		*Form Approved OMB No. 0704–0188*

Public reporting burden for this collection of information is estimated to average 1 hour per response, including the time for reviewing instruction, searching existing data sources, gathering and maintaining the data needed, and completing and reviewing the collection of information. Send comments regarding this burden estimate or any other aspect of this collection of information, including suggestions for reducing this burden, to Washington headquarters Services, Directorate for Information Operations and Reports, 1215 Jefferson Davis Highway, Suite 1204, Arlington, VA 22202-4302, and to the Office of Management and Budget, Paperwork Reduction Project (0704–0188) Washington DC 20503.

1. AGENCY USE ONLY *(Leave blank)*	2. REPORT DATE March 2012	3. REPORT TYPE AND DATES COVERED Master's Thesis
4. TITLE AND SUBTITLE A Climatological Study of Hurricane Force Extratropical Cyclones		**5. FUNDING NUMBERS**
6. AUTHOR(S) Razaak O. Laiyemo		
7. PERFORMING ORGANIZATION NAME(S) AND ADDRESS(ES) Naval Postgraduate School Monterey, CA 93943–5000		**8. PERFORMING ORGANIZATION REPORT NUMBER**
9. SPONSORING /MONITORING AGENCY NAME(S) AND ADDRESS(ES) N/A		**10. SPONSORING/MONITORING AGENCY REPORT NUMBER**

11. SUPPLEMENTARY NOTES The views expressed in this thesis are those of the author and do not reflect the official policy or position of the Department of Defense or the U.S. Government. IRB Protocol number ___N/A____.

12a. DISTRIBUTION / AVAILABILITY STATEMENT Approved for public release; distribution unlimited	12b. DISTRIBUTION CODE A

13. ABSTRACT (maximum 200 words)

Using data compiled by the National Weather Service Ocean Prediction Center, a hurricane force extratropical cyclone climatology is created for three cold seasons. Using the criteria of Sanders and Gyakum (1980), it is found that 75% of the 259 storms explosively deepened. The frequency maximum in the Atlantic basin is located to the southeast of Greenland. In the Pacific, two maxima to the east of Japan are identified.   These results are in good agreement with previous studies, despite different cyclone subgroups, datasets, and methodologies. Composite analyses illustrate the hurricane force wind subgroup of extratropical cyclones, similar to other extratropical cyclones, form in regions of anomalously strong baroclinicity and begin to intensify upstream of an upper-level positive PV anomaly. By the end of the 24-hour period of maximum deepening rate, the composite storm structure appears nearly vertically stacked. Shortly after this time, the storm begins to weaken. There is some indication that diabatic processes serve as an additional energy source. Brief examination of predictability using ECMWF and NCEP ensemble data to analyze two randomly-selected storms indicate significant features like storm track and intensity are not properly captured by the ensemble prediction systems.

14. SUBJECT TERMS Extratropical Cyclones, Hurricane, Vorticity, Climatology, Explosive Deepening, Composite, Anomaly, and Ensemble.			**15. NUMBER OF PAGES** 105
			16. PRICE CODE
17. SECURITY CLASSIFICATION OF REPORT Unclassified	**18. SECURITY CLASSIFICATION OF THIS PAGE** Unclassified	**19. SECURITY CLASSIFICATION OF ABSTRACT** Unclassified	**20. LIMITATION OF ABSTRACT** UU

NSN 7540–01-280–5500

Standard Form 298 (Rev. 8–98)
 Prescribed by ANSI Std. Z39.18

THIS PAGE INTENTIONALLY LEFT BLANK

A CLIMATOLOGICAL STUDY OF HURRICANE FORCE EXTRATROPICAL CYCLONES

Razaak O. Laiyemo
Lieutenant Commander, United States Navy
B.S., Jacksonville University, 2002

Submitted in partial fulfillment of the
requirements for the degree of

MASTER OF SCIENCE IN METEOROLOGY AND PHYSICAL OCEANOGRAPHY

from the

**NAVAL POSTGRADUATE SCHOOL
March 2012**

Author: Razaak Laiyemo

Approved by: Richard Moore
                 Thesis Advisor

                 Wendell Nuss
                 Second Reader

                 Wendell Nuss
                 Chair, Department of Meteorology

THIS PAGE INTENTIONALLY LEFT BLANK

ABSTRACT

Using data compiled by the National Weather Service Ocean Prediction Center, a hurricane force extratropical cyclone climatology is created for three cold seasons. Using the criteria of Sanders and Gyakum (1980), it is found that 75% of the 259 storms explosively deepened. The frequency maximum in the Atlantic basin is located to the southeast of Greenland. In the Pacific, two maxima to the east of Japan are identified. These results are in good agreement with previous studies, despite different cyclone subgroups, datasets, and methodologies. Composite analyses illustrate the hurricane force wind subgroup of extratropical cyclones, similar to other extratropical cyclones, form in regions of anomalously strong baroclinicity and begin to intensify upstream of an upper-level positive PV anomaly. By the end of the 24-hour period of maximum deepening rate, the composite storm structure appears nearly vertically stacked. Shortly after this time, the storm begins to weaken. There is some indication that diabatic processes serve as an additional energy source. Brief examination of predictability using ECMWF and NCEP ensemble data to analyze two randomly-selected storms indicate significant features like storm track and intensity are not properly captured by the ensemble prediction systems.

THIS PAGE INTENTIONALLY LEFT BLANK

TABLE OF CONTENTS

THIS PAGE INTENTIONALLY LEFT BLANK

LIST OF FIGURES

THIS PAGE INTENTIONALLY LEFT BLANK

LIST OF TABLES

THIS PAGE INTENTIONALLY LEFT BLANK

LIST OF ACRONYMS AND ABBREVIATIONS

2D	2-Dimension
3D	3-Dimension
CCB	Cold Conveyor Belt
DI	Dry Intrusion
DJF	December January February
ECMWF	European Center for Medium-Range Weather Forecasts
ERA	European Center for Medium-Range Weather Forecasts Re-Analysis
G	Gale – for winds from 34–47 knots
GMT	Greenwich Meridian Time
H	Hurricane – for winds greater than 63 knots
JJA	June July August
Km	Kilometers
kts	Knots
L	Low–for winds less than 43 knots
LHR	Latent Heat Release
MAM	March April May
NCEP	National Center for Environment Predictions
NMC	National Meteorological Center
NWS	National Weather Service
OPC	Ocean Prediction Center
S	Storm-for winds from 48 to 63 knots
SLP	Sea Level Pressure

SON   September October November

SST   Sea Surface Temperature

TIGGE   Thorpex Interactive Grand Global Ensemble

WCB   Warm Conveyor Belt

THIS PAGE INTENTIONALLY LEFT BLANK

ACKNOWLEDGMENTS

THIS PAGE INTENTIONALLY LEFT BLANK

I.   INTRODUCTION

A.   MOTIVATION

It is well known that hurricanes generate strong and damaging winds. Most are familiar with the Saffir-Simpson Scale, which aims to characterize the intensity of hurricanes, primarily based on the magnitude of sustained low-level winds.   For example, a storm system is determined to have reached hurricane status once sustained winds reach 64 knots (Category One on the Saffir-Simpson Scale).It is less commonly known that extratropical cyclones are also capable of generating hurricane-force low-level winds.   Using model forecast data and Quick Scatterometer (QuikSCAT) satellite data over the ocean to estimate surface wind speed, forecasters from the National Weather Surface Ocean Prediction Center provide in real-time 6-hourly analyses for the North Atlantic and North Pacific ocean basins that include warnings of strong regional winds (gale, storm and hurricane-force winds).

An example of a North Atlantic storm that was associated with hurricane-force winds occurring in February 2007 is presented in Figure 1.   Coincident images of the infrared satellite and QuikSCAT retrieved surface wind direction and speed data are shown.   A large region of greater than hurricane-force winds is captured in the QuikSCAT data (red wind barbs indicate wind speeds greater than 63 knots).   In this particular case, hurricane-force winds were sustained during a 30-hour period of time.
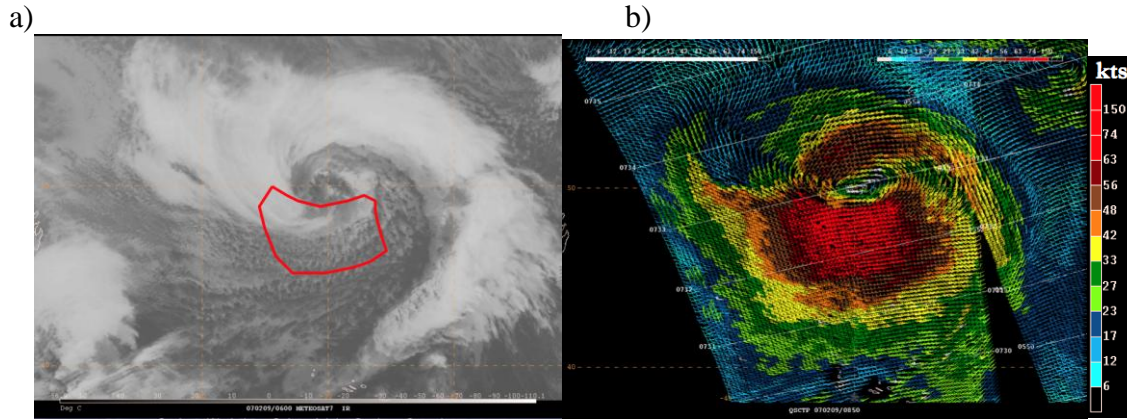
Figure 1. Hurricane-force extratropical cyclone at 06 UTC February 9, 2010: a) infrared brightness temperature from Meteosat; and b) QuikSCAT wind direction and speed. The red box in a) outlines the region of hurricane strength winds identified in b).

Compiling individual cases, it is possible to examine the location and frequency of hurricane-force extratropical cyclones. Data from the years 2000–present currently exist. A climatology for the years 2000 through 2007 illustrates that the number of hurricane-force extratropical cyclones is quite significant: approximately 500 storms, nearly evenly split between the Pacific and Atlantic basins, are identified. The 7-year average storm frequency and location for the Atlantic and Pacific basins are presented in Figure 2. On average, more than 50 such storms per year were found during this time period. However, this number almost assuredly underestimates the actual amount: the number-per-year occurrence has risen throughout the 2000 to 2008 time period, primarily due to forecaster familiarity, data availability and improved QuikSCAT algorithms. In looking at the 2006–2007 and 2007–2008 cold season tallies, the average storms-per-season is nearly 100.

Winds of such magnitude are capable of causing significant damage to property and life, both over land and sea. Furthermore, given the proclivity for the strongest extratropical cyclones to form and intensify over the ocean surface where there are few in-situ measurements, a grave danger is specifically posed for seafaring crafts (both military and civilian). This point is highlighted by the

inclusion of major shipping routes in Figure 2 (yellow lines). It is clear that these intense extratropical cyclones pose a danger to the ships in their path and, thus, the proper forecasting of storm path and intensity is extremely important for damage mitigation.

However, an additional repercussion of the oceanic nature of the strongest storms (Sanders and Gyakum 1980) and the concomitant lack of observational data is the impact on numerical weather prediction (NWP): due at least in part to initial condition errors, NWP models are unable to consistently forecast accurate wind strength, which is often underestimated, leading to 6–8 fold underestimates in damage (Browning 2003). The overall effect is inadequate preparedness or grossly disproportionate damage mitigation efforts, especially for storms that track over land.
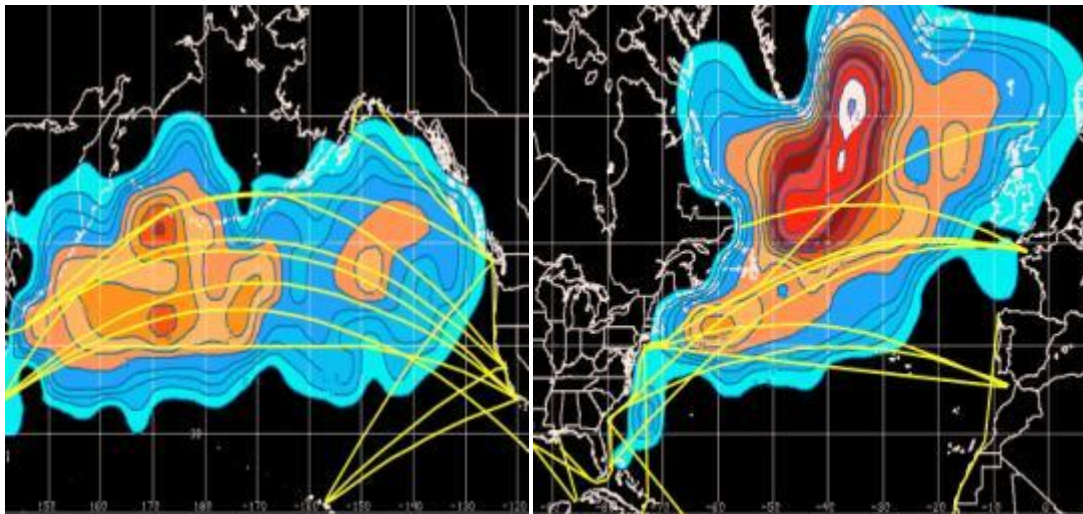
Figure 2.   2000–2007 annual-average hurricane force extratropical cyclone for the North Pacific (left) and the North Atlantic (right) Oceans (contour interval of 1 storm) Yellow contour represent major shipping lanes. (From Sienkiewicz et al. (2008)).

In Europe alone, according to Robert Muir Woods in a lecture to the Royal Meteorological Society in December of 2001, damages due to strong surface winds from extratropical cyclones since 1985 have costs over 24 billion Euros (Browning 2003).

In December of 1999 alone, three violent extratropical cyclones *Anatol, Lothar* and *Martin*, caused damages worth over 13 billion Euros, costing more than 130 lives (Ulbrich et al. 2000), and leaving over 1 million people without electricity (Browning 2003).

Anatol, an extratropical cyclone that occurred between the 2nd and 4th of December, developed of the central and north Atlantic south of Greenland. Anatol's largest winds speeds occurred south of the cyclone core in a belt reaching from the German and Southern Danish North seacoast to Copenhagen and the Polish Baltic seacoast. Wind gusts exceeding 25 m s^{-1} were observed over Denmark during the eight-hour period from 1400 to 2200 GMT (Ulbrich et al. 2000).

Lothar, an extratropical cyclone that developed off the North American coast at about 35° N, occurring from the 24th–27th of December 1999, wreaked havoc and destruction from northwestern France to southern Germany and Switzerland (Ulbrich et al. 2000). Gusts reaching wind speeds of almost 50 m s^{-1} were recorded at the Paris-Orly airport. In Germany and Switzerland persistent violent gusts of over 41 m s^{-1} and 37 m s^{-1} respectively were recorded. The winds uprooted countless of tress causing losses in forestry (Ulbrich et al. 2000).

Martin, another extratropical cyclone just a day after Lothar occurred from the 25th–28th of December, and exhibited wind gusts of 36 m s^{-1} over western France (Ulbrich et al. 2000)

B.   PREVIOUS RESEARCH

1.   General Overview of Extratropical Cyclones

Extratropical cyclones are synoptic scale low-pressure weather systems that occur outside of the tropics. Their primary energy source comes in the form of a baroclinic zone (meridional temperature gradient). While not a necessary ingredient, diabatic processes can serve as an additional energy source.

a. Baroclinic Zone

Due to the inhomogeneity of radiative heating, there is a surplus of energy in the tropics and a deficit near the poles. The result is relatively warm air at low latitudes and relatively cold air at higher latitudes, representing a meridional temperature gradient. In a time-mean sense, the meridional temperature gradient is maximized in the midlatitudes and is often referred to as the polar front. In essence, the polar front is the transition zone between air masses of differing density and it is the ambient baroclinicity that represents the available potential energy (APE) for extratropical cyclones.

To see how baroclinicity might serve as an energy source for an extratropical cyclone, a simple thought experiment proves insightful. An unperturbed baroclinic zone can be likened to the state shown in Figure 3a where the two fluids of dissimilar densities are separated by a barrier. Once the barrier is removed, the APE in the form of the density contrast will be converted to kinetic energy (KE) of motion as the heavier fluid seeks the bottom of the contained and the lighter fluid rises to the top surface.
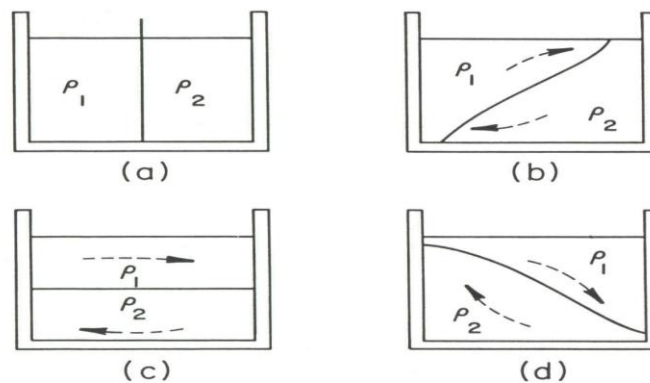
FIG. 4.13   A schematic illustration of available potential energy and its relationship to kinetic energy. (a) Initial state: a barrier separates immiscible fluids of differing density, ρ, where $\rho_2 > \rho_1$. The barrier is removed and gravity accelerates the flow (b) until maximum velocity (maximum kinetic energy) is reached (c). At (c) the potential energy is a minimum, but not zero. The change in potential energy between (a) and (c) is the available potential energy. (d) The current overshoots, the deceleration converts kinetic into potential energy.

Figure 3.   Schematic of a). 2 fluids of dissimilar densities separated by a barrier. b). barrier removed and gravity accelerates the fluids until maximum velocity is reached. APE is converted to KE. c). APE is at a minimum. d). the current overshoots, the deceleration coverts KE to PE. (From *Global Atmosphere Circulations*, by R Grotjahn).

The equivalent process in the atmosphere is shown schematically in Figure 4. The background state is represented by the polar front separating two air masses: a cold polar air mass to the north and a warm tropical air mass to the south. Via some mechanism, a low-pressure center forms along the boundary (Figure 4b). Low surface pressure induces cyclonic flow and the polar front is perturbed from its initial state.
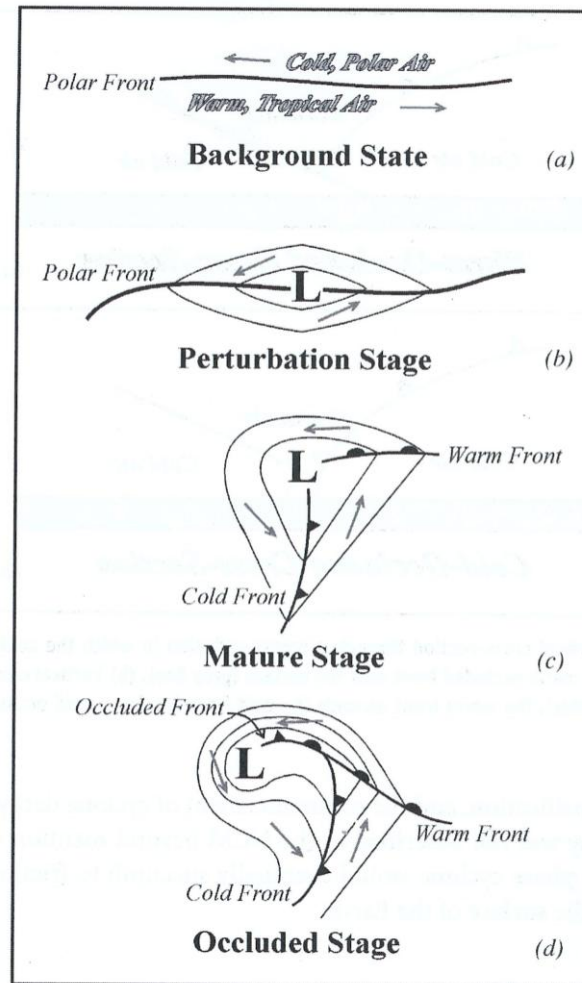
Figure 4. Evolution of a midlatitude cyclone according to Norwegian Cyclone Model. (a) The polar front as a background state. (b) The initial cyclonic perturbation. (c) the mature stage. (d) The occluded stage. The think solid line are isobars of the sea–level pressure and the arrows are the surface winds vectors. (From Martin (2006)).

In response to the cyclonic flow, cold and warm air advection begins to take place. The system intensifies due to a positive feedback between upper-level divergence and low-level temperature advection. This occurs as long as the storm system exhibits the characteristic westward tilt with height in terms of the trough / ridge pattern and eastward tilt with height of the temperature perturbation (shown schematically in Figure 5). In this setup the warm air advection that occurs to the east of the surface pressure low serves to increase the height of the middle troposphere (ridge building) while the cold air advection lowers the middle tropospheric height (trough deepening) (Martin 2006). This amplification of the wave serves to increase upper-level divergence, which in term, deepens the low and increases the magnitude of the low-level temperature advection.
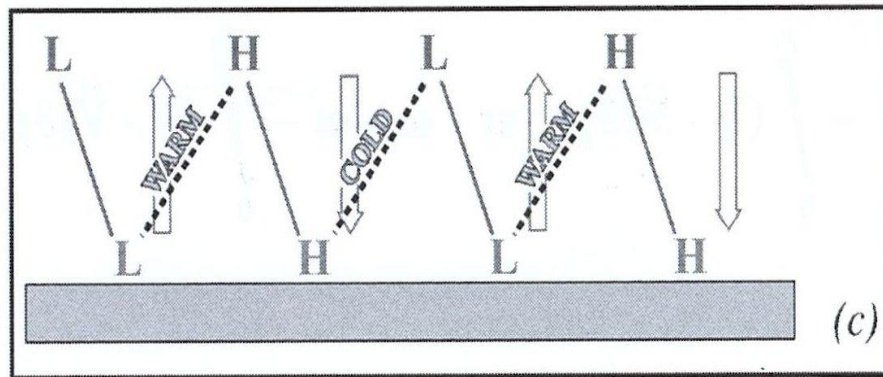
Figure 5. Vertical structure of a developing midlatitude cyclone. Upper tropospheric lows and highs are displaced to the west with the height. Thick dashed lines are thermal axes, which tilt slightly to the east with height. Note that warm air is ascending and cold air is descending in this wave train. (From Martin (2006)).

As the occlusion process occurs, the mechanism for the positive feedback described above is removed. The low-level temperate gradient is minimized, as the warm air mass now resides above the cold air mass. The final state exhibits a temperature gradient that is much less than that of the original background state. The APE was converted into KE of motion and heat was transported poleward.

b. Convergence and Divergence

The surface pressure tendency equation is provided below.

$$\frac{\partial Ps}{\partial t} \approx \int_0^{Ps} (\nabla \cdot \vec{V}) dp$$

P_s is the surface pressure and V is the horizontal velocity vector. The equation predicts that the surface pressure tendency at a given point is a consequence of the total divergence of mass in a vertical column of atmosphere (Martin 2006). In the context of an extratropical cyclone characterized by upper-level divergence and low-level convergence in the vicinity of the storm center, the surface pressure will drop if the magnitude of the divergence is larger than that of the convergence.

As an upper level trough approaches a baroclinic zone, the height falls to the west of the surface low leads to a positive, mid-tropospheric geostrophic vorticity tendency there, while the height rises to the east of the SLP minimum are associated with a negative, mid-tropospheric geostrophic vorticity tendency there (Martin 2006). Positive vorticity is advected eastward by the zonal flow, which is associated with upward vertical motion. As discussed above, a westward tilt with height of the trough axis is indicative of an intensifying extratropical cyclone. The more intense the temperature advection, the more the building (deepening) of the mid-tropospheric ridge (trough), the more the upward vertical motion, until the APE is converted to KE and a more stable stratification is reached.

c. Latent Heat

As a cyclone starts to develop, the cyclonic flow of air at the lower levels serves to bring warm air poleward on the eastern side of the surface low. The warm air advection coupled with the ascent of moist air further enhances warming on the eastern side of the surface low due the latent heat release (LHR) during condensation and cloud formation (Martin 2006). According to Martin

(2006), this process further intensifies the low-level temperature gradient and consequently increases the magnitude of the warm air advection there. The LHR to the east of the low-pressure center increase the geopotential height in the middle and upper tropospheric regions, building a ridged and shortening the wavelength between the upstream trough and downstream ridge. As a result of the shortening of the wavelength, the magnitude of the positive vorticity advection downstream of the trough axis is intensified creating more upward vertical motion, and a positive feedback loop (Martin 2006). In conjunction with building the midlevel ridge downstream, the generation of LHR through diabatic heating creates a low-level positive potential vorticity (PV) anomaly, which enhances upward vertical motion.

In a study of the role of latent heat release in explosive cyclogenesis by Reed et al. (1988), numerical experiments were conducted on operational forecasts on three cases of explosive cyclogenesis. It was found that latent heat released accounted for 40%–50% of the deepening in the well-forecasted cases (two of the three cases). In the first well-forecasted case, the experiment showed that the moist model best represented the explosive deepening that occurred by predicting deepening of 35 hPa in a 24-hour period. The dry model run predicted a central pressure that was 16 hPa higher than the moist run. The dry baroclinicity accounted for 54% of the deepening while the moist run accounted for the remaining 46% (Reed et al. 1988).

The study of the second successful forecast exhibited similar results. The moist run accounted for 41% of the deepening while the dry run predicted a deepening that was 19 hPa less than the moist run. The results as to why the third forecast failed were inconclusive, but some evidence pointed to poor analysis that failed to fully capture the high moisture content and low static stability of the warm sector air that was ingested into the heart of the storm (Reed at al. 1998). As a whole, the experiments show that LHR served as an energy source that aids in the intensification of extratropical cyclones.

d.   Cloud Formation and Coherent Air Streams

In order to provide insight into the evolution of the observed cloud pattern associated with extratropical cyclones, Carlson (1980) analyzed the airflow through a midlatitude disturbance in a relative-wind isentropic system. He was able to identify three coherent air streams in which air parcels share a similar dynamic and thermodynamic evolution. The three primary air streams are illustrated in Figure 6.
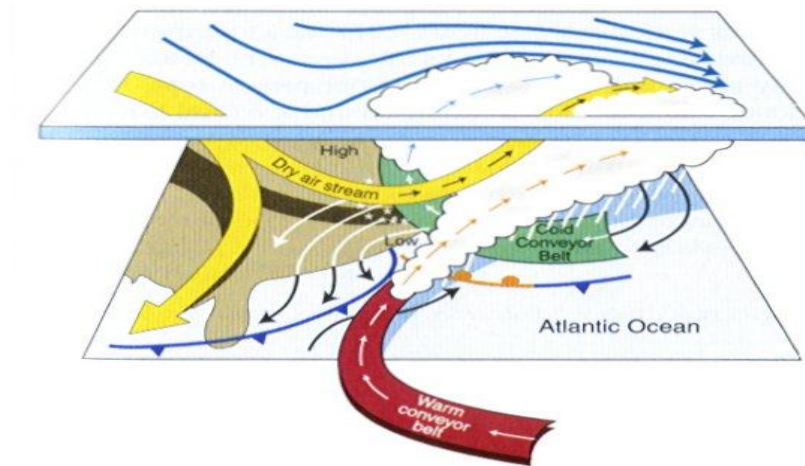
Figure 8.24   Three-dimensional wind flow through a Northern Hemisphere frontal cyclone, according to the conveyor belt model.
Source: From "Snowstorms Along the NE Coast of US" by P. W. Kocin and L. W. Uccellini in *American Meteorological Society*, 1990. Copyright © 1990. Reprinted by permission of the American Meteorological Society.

Figure 6.   Schematic of coherent airstreams found in extratropical cyclone. Schematic depicts the warm conveyor belt (WCB), cold conveyor belt (CCB), and dry intrusion. Also shows pressure levels at different locations. (From *Meteorology*, by Danielson, Levin and Abrams).

The Warm Conveyor Belt (WCB) represents the main source of warm, moist air that feeds the cyclone. It originates in the warm sector of the cyclone at low-levels and flows poleward parallel to the cold front.   As the flow approaches the warm front, it begins to ascend with its strongest rise over the warm front, in the area of strongest warm air advection, and turns anti cyclonically in the upper troposphere.

10

The Cold Conveyor Belt (CCB) begins to the northeast of the low-pressure center of the storm. This air stream flows westward, on the cold side of the warm front, below the WCB, toward the center of the low-pressure circulation. The air becomes saturated through a combination of precipitation falling into the CCB from the WCB above and slow ascent from the boundary layer to the mid-troposphere north of the low center. The flow eventually rises and turns anticyclonically into the upper tropospheric ridge ahead of the developing cyclone.

The Dry Intrusion (DI) begins at upper-levels and sinks behind the cold front. It parallels the WCB and rises over the CCB. The dry intrusion area is easily identifiable on water vapor and satellite imagery due to its distinct dryness.

The result of these three coherent air streams is the comma-shape cloud pattern of an extratropical cyclone observed in satellite imagery. The WCB is responsible for the clouds associated with the southwesterly flow along the cold front and north of the warm front that form the comma tail and the body. The CCB creates the middle level clouds situated west and north of the surface low, forming the westward extension of the comma head. The distinctly sharp edge of the cloud pattern on the west edge of the comma tail, as well as the northern and northwestern portion of the comma head comprising of the anticyclonically curved cirrus shield northeast of the low, is associated with the DI (Carlson 1880).

Typically, strong surface winds in an extratropical cyclone are associated the WCB and CCB as described above. It is possible for winds of hurricane strength to be sustained for a number of days.

2. Explosive Deepening Cyclones "Bomb"

An explosively deepening extratropical cyclones is characterized or defined as a storms that exhibits a sea level central pressure fall of at least 1 hPa h^{-1} for 24 hours at latitude 60°N (Sanders and Gyakum 1980). This necessary threshold is termed one Bergeron. In order to correct for latitude, a

geostrophically equivalent rate is obtained for arbitrary latitudes Ø (Sanders and Gyakum 1980).

$$1 \text{ Bergeron} = 24 \times \left(\frac{\sin \text{Ø}}{\sin 60} \right)$$

The value of 1 Bergeron varies from 28 hPa at the pole to 12 hPa at 25° north (Sanders and Gyakum 1980). Sanders and Gyakum (1980) called storms meeting or exceeding one Bergeron "bombs" (Sanders and Gyakum 1980).

Using data from the National Meteorological Center (NMC) and selecting cold seasons from October 1976–March 1977, and September–March of 1977 and 1978, respectively, Sanders and Gyakum (1980) created a climatology of bombs. The raw deepening was obtained by comparing the 1200 GMT central pressures on successive days. The frequency and location of the 267 bomb storms recorded during the three cold seasons is presented in Figure 7. The bombs occurred primarily in a maritime environment with enhanced frequencies occurring in the westernmost portions of the Atlantic and Pacific Oceans. They were found to predominantly occur $5–10^{\circ}$ poleward of the zone of maximum winter initial cyclogenisis frequency shown by Petterssen (1956, p.267) and within or just north of the warm waters of the Gulf Stream and the Kuroshio respectively (Sanders and Gyakum 1980).
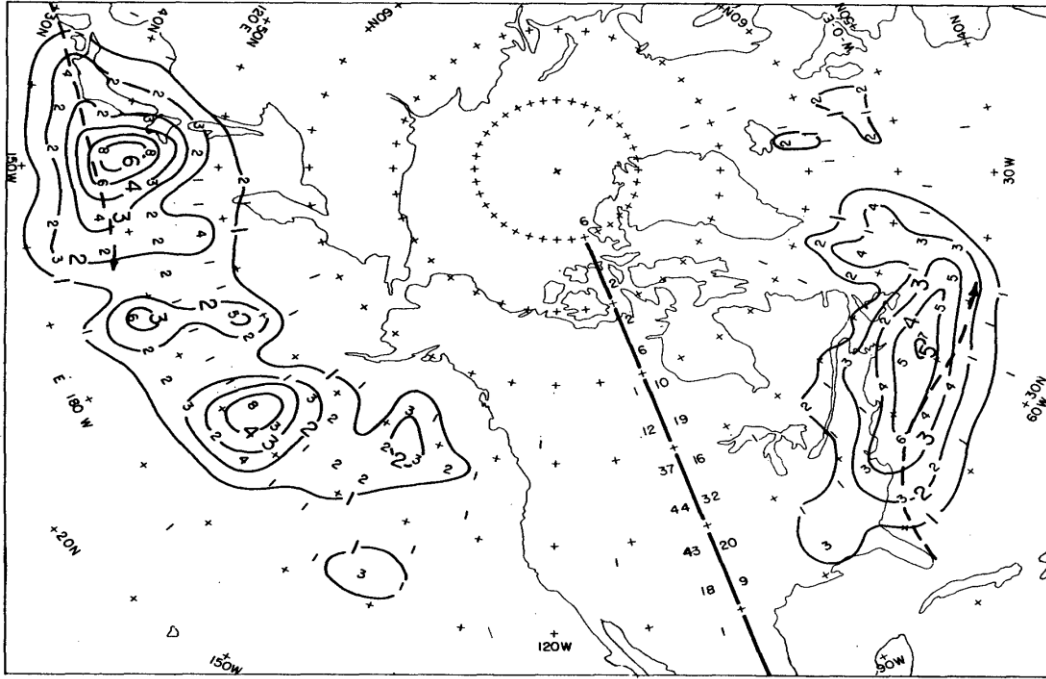
Figure 7. Distribution of bomb events during three cold seasons. Raw non-zero frequencies appear in each 5° x 5° quadrilateral of latitude and longitude. Isopleths represent smoothed frequencies, obtained as one-eighth of the sum of four times the raw central frequency plus the sum of the surrounding raw frequencies. The column of numbers to the left and right of the heavy line along longitude 90° W represents, respectively the normalized frequency for each of the 5° latitude belt in the Pacific and Atlantic regions, using a normalization factor of (cos 42.5/cos ϕ). (From Sanders and Gyakum (1980)).

Tracking the mobile 500mb trough, they observed that each bomb event occurred when the low-pressure center was to the north east of the 500mb trough. Dynamically this area is an area of maximum positive vorticity advection, which signifies divergence aloft and convergence at the surface. Sea surface temperatures (SST) were examined to determine if there was a direct relationship between SSTs and bombs. Figure 8 shows the plot of SST against the normalized deepening rate. They found that bombs occurred through a wide range of SST's, implying a lack of sensitivity to SSTs (in contrast to tropical cyclones).

13
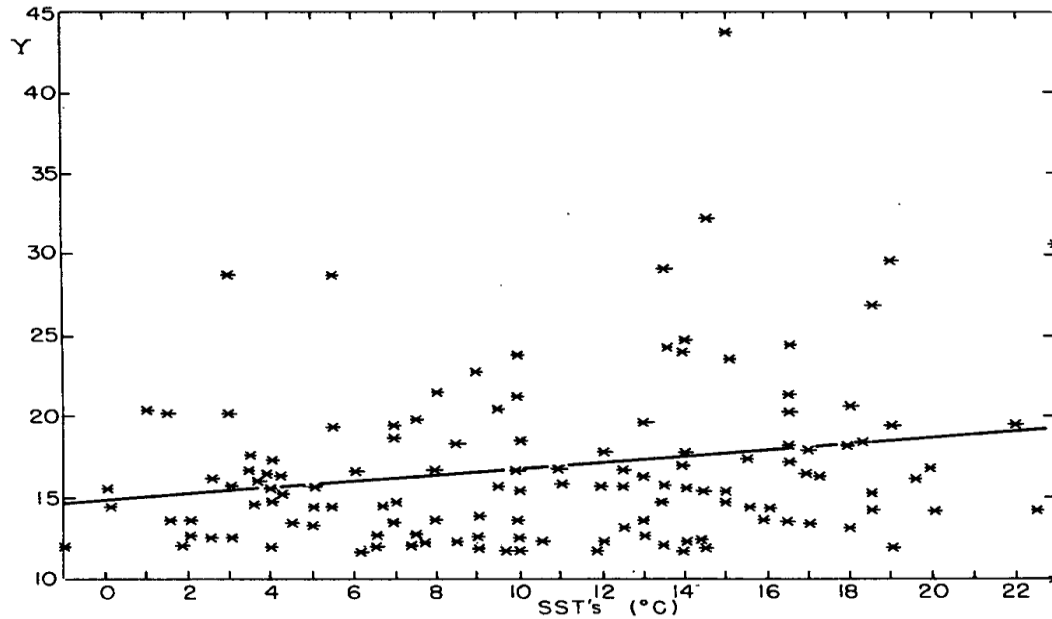
Figure 8. Plot of all available bombs 1979–79 bombs (indicated by asterisk) with respect to its underlying SST and its subsequent 12 h central pressure fall. The dark line shows the least square fit. (From Sanders and Gyakum (1980)).

In 1986, Rogers and Bosart conducted a composite study of explosively deepening oceanic cyclones. For composite construction, meteorological data from a North Atlantic and Pacific weather ships for nine cold seasons (October–April) from 1965–1974 were used. For central pressure compilations and bomb calculations, data from the National Meteorological Center NMC were used. They conducted their composite analysis in temporal stages, defining the stages as follows:

- Incipient Stage—the period commencing from initial formation of a low pressure area

- Explosive Stage—the period during which rapid deepening is occurring, defined as pressure falls > 12 hPa (12 h)⁻1

- Mature Stage—the period during which (i) rapid central pressure ceases to fall (ii) the central pressure and areal extent of the cyclone's circulation remain quasi-steady.

14

- Decaying Stage—the period during which there is noticeable increase in the storm's central pressure and decrease in the storm's intensity. This state continues until the cyclone loses its identity.

They concluded that explosively deepening cyclones evolve an incipient circulation that was confined to the lower troposphere. The cyclone subsequently developed into a deep intense vortex characterized by strong baroclinicity, and strong low and midlevel accent to the north and east of the cyclone, and lower tropospheric conditional instability near and to the southeast of the cyclone center.

3.   Statistical Analysis of Explosive Cyclones

Roebber (1984) conducted a statistical analysis of extratropical cyclone deepening rates, including all surface lows. He also expanded the bomb climatology of Sanders and Gyakum (1980) to include the 1979–1982 cold seasons. The idea was that by including all storms in the compilation of a cyclone climatology, a better relationship between rapid deepeners and non-rapid deepeners can be identified and show that other mechanism(s) are factors in rapid deepening cyclones which could promote further research in the area of explosive cyclogenesis.
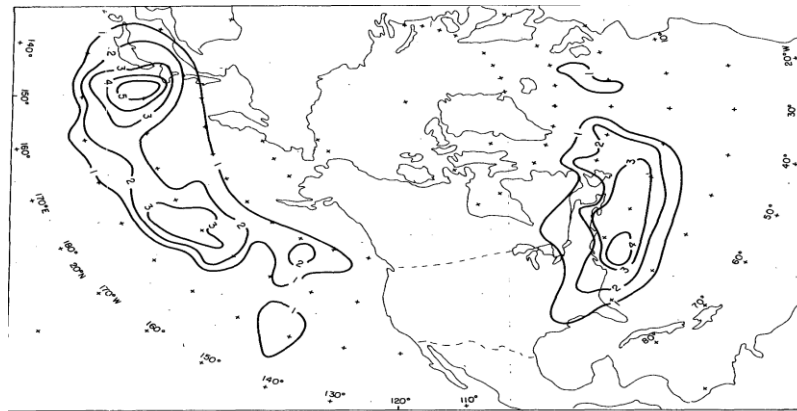
Figure 9. Geographic distribution of 1976–79 bombs (From Roebber (1984)).
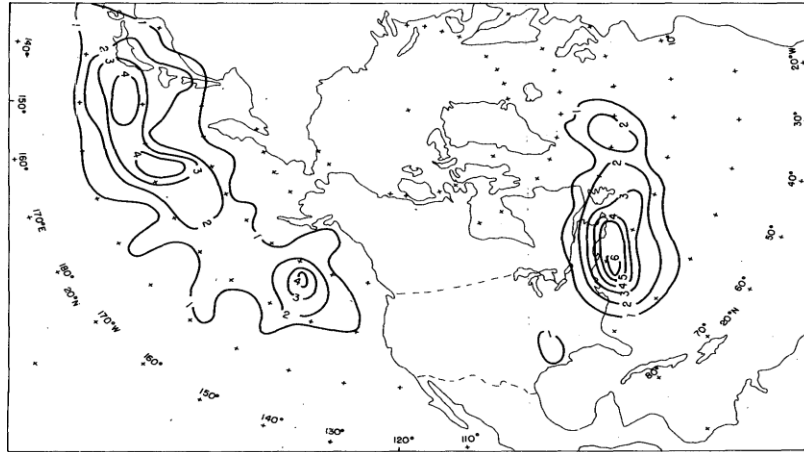
Figure 10.   Geographic distribution of 1979–82 bombs (From Roebber (1984)).
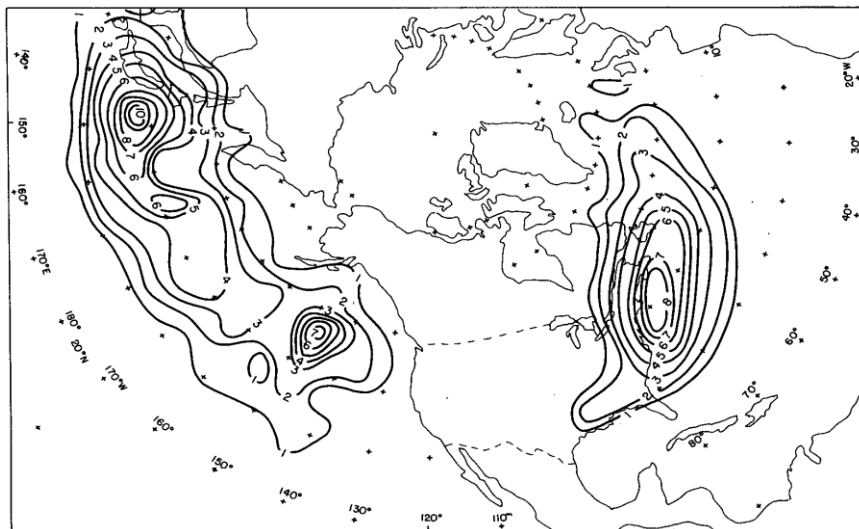
Figure 11.   Geographic distribution of 1976–82 bombs (From Roebber (1984)).

The geographic distribution of bombs for the 1976–1979 , 1979–1982, and 1976–1982 cold seasons are presented in Figures 9–11, respectively. Roebber's (1984) study showed that the preferred regions of explosive cyclone development are primarily baroclinic zones, which is very consistent with Sanders and Gyakum's study (1980). The frequency plots are virtually the same between the two studies showing maxima in the same regions of the Atlantic and Pacific

16

Oceans. In addition, Roebber determined that in a similar fashion as non-explosive cyclones, explosive cyclones exhibit a relationship to the upper level flow (500 hPa) which is consistent with Sanders and Gyakum (1980). The study concluded that the statistical analysis also supported the conclusion of the follow on study by Gyakum (1983b) and Bosart (1981) that there are mechanism(s) coupled with the baroclinic process that cause explosive deepening of cyclones. The mechanism(s) could include processes like latent heat release during cumulus convection.

C.   RESEARCH OBJECTIVES AND THESIS ORGANIZATION

The overarching goal of this research project is to better understand the general characteristics of hurricane-force extratropical cyclones. Via the examination of a novel dataset created by the National Weather Service Ocean Prediction Center, a three-fold methodology is employed. The first encompasses a climatological analysis of storm frequency, location, and evolutionary characteristics. These data are presented in Section 3, after the study data and methodology are outlined in Section 2. The second involves the compositing of relevant dynamical features in an effort to gain insight into the important dynamical processes at work (Section 4). Finally, we will briefly examine the predictability of two such storms through the utilization of ensemble prediction data (Section 5). Finally, study conclusions and a general discussion are provided in Section 6).

THIS PAGE INTENTIONALLY LEFT BLANK

II. DATA AND METHODOLOGY

A. DATA

1. National Weather Service Ocean Prediction Center Hurricane-Force Database

The primary source of storm data comes from the National Weather Service (NWS) Ocean Prediction Center (OPC). Since 2000, the OPC has catalogued information regarding hurricane-strength extratropical cyclones from their 6-hourly analyses. An example of one such analysis for the Atlantic basin on 6th of March 2012 is provided in Figure 12.
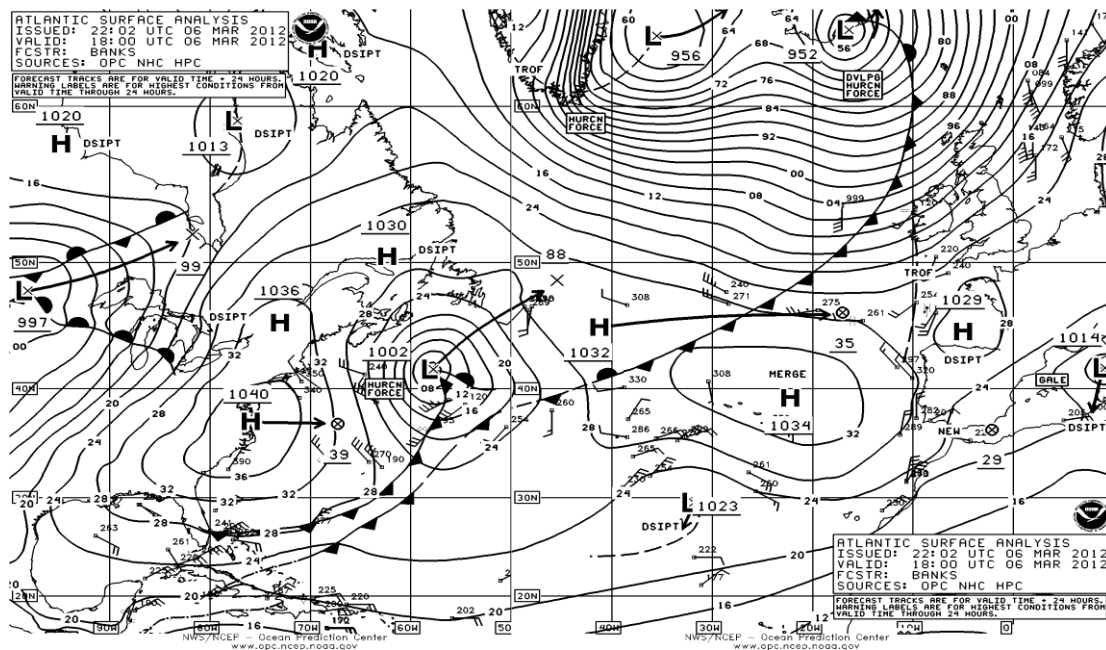
Figure 12.   Surface analysis issued by OPC for hurricane force winds warning in the Atlantic. Issued 2202 UTC 06 Mar 2012.

At this time, two hurricane-force extratropical cyclones are identified: one located east of Nova Scotia at approximately 42°N and 57°W and the other east of Greenland at approximately 65°N and 25°W. A third storm was characterized as a developing hurricane-force storm system has a low-pressure center north-west of England at approximately 66°N and 16°W.

The database that was acquired from the OPC includes all hurricane-force extratropical cyclones that occurred from 2001–2009. A storm is included in the database if there is at least one 6-hourly analysis that includes a hurricane-force reading. A storm is tracked based on threshold wind values:

- Low (L): less than 34 knots
- Gale (G): 34 to 47 knots
- Storm (S): 48 to 63 knots
- Hurricane (H): greater than 63 knots

The dataset includes the storm name, position (latitude and longitude), year, month, day, hour, minimum sea-level pressure, and wind category (L, G, S, H). The dataset is recorded in GMT and compiled every six hours (0000, 0600, 1200, and 1800).

While data has been catalogued since December 2000, the detection methodology has evolved with time. Improvements in forecaster familiarity, data availability and improved QuikSCAT algorithms have impacted the ability of the OPC to identify cases. Figure 13 illustrates this point. It is apparent that storm detection has significantly increased in response to changes in the methodology. In May of 2004 the QuikSCAT's resolution was improved from 25 Km to 12.5 Km and Figure 13 shows increases in hurricane force wind detection from cold seasons 2004–2006 in both the Atlantic and Pacific basins. In 2006, the wind speed detection algorithm was improved and once again, Figure 13 shows the corresponding increase in hurricane force wind detection.
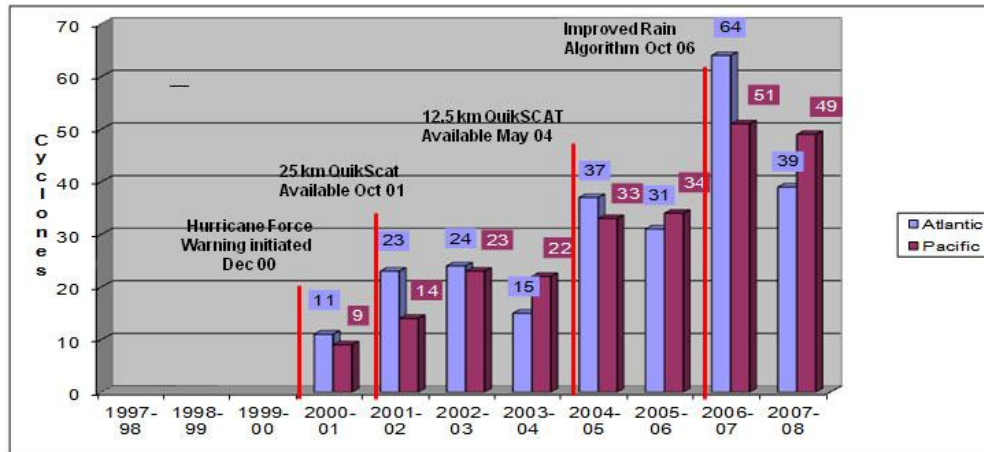
Figure 13.　Storm frequency as a function of cold seasons and changes in the detection methodology. (From Sienkiewicz et al. (2008)).

To promote consistency in our results, we focus on the period after the introduction of an improved wind algorithm and rain flag in October 2006.　In addition, given the relative lack of storms during the warm season (see Figures 14 and 15), we only examine data for the cold season (defined as October through March) of each year.　Due to the failure of QuikSCAT in late 2009, there are three cold seasons that were compiled with a consistent methodology (2006–2007, 2007–2008, 2008–2009).
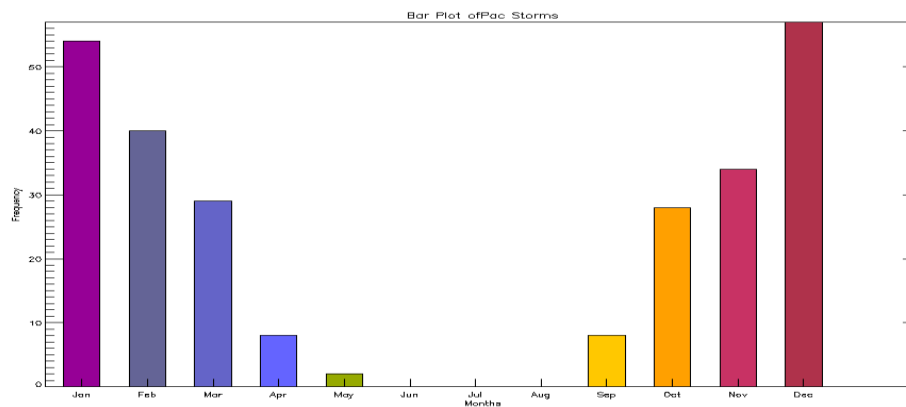
Figure 14.　Total number of hurricane force wind extratropical cyclone by months in the Pacific basin. Most of the storms occur from October through March.

21
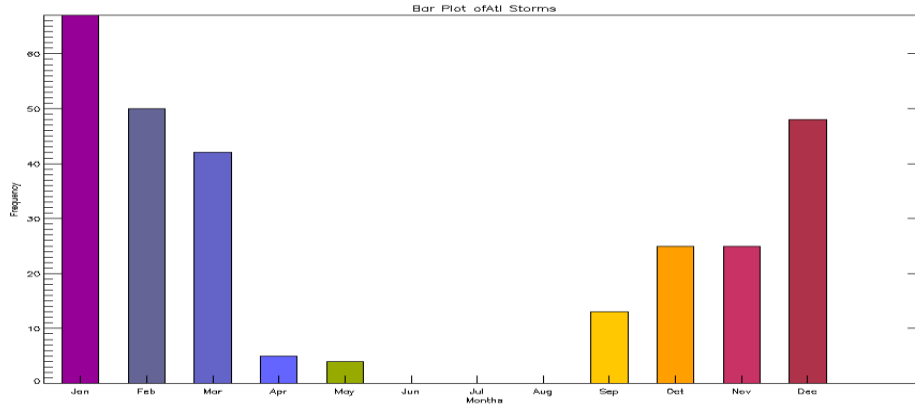
Figure 15.   Total number of hurricane force wind extratropical cyclone by months in the Atlantic basin . Most of the storms occur from October through March.

2.   European Center for Medium-Range Forecast Interim Database

The European Center for Medium-Range Forecast Interim database, also knows as ERA-interim, is a global database that covers from January 1989 on to the present. We used a resolution of 1 X 1 degree and 60 vertical levels of meteorological data. The database includes 6-hourly surface parameters, describing weather as well as ocean-wave and land-surface conditions, and 6-hourly upper-air parameters covering the troposphere and stratosphere The ERA-Interim archive currently contains 6-hourly gridded estimates of three-dimensional (3D) meteorological variables, and 3-hourly estimates of a large number of surface parameters and other two-dimensional (2D) fields, for all dates from 1 January 1989 (D. P. Dee et al. 2011). From this database we created a number of meteorological fields to include: temperature, vorticity, specific humidity, liquid water content, potential vorticity, and potential temperature for the composite analysis of hurricane force extratropical cyclones.

B.   METHODOLOGY

1.   Climatology

Based on the OPC database, the genesis of a hurricane force extratropical cyclone begins once the observed wind speed is greater than the L

wind threshold of 34 kts. The lifecycle of the storm would be from this point until the cyclone's wind speeds become less than 34 kts. We focused our study on the cold season of 2006–2007, 2007–2008 and 2008–2009 (October–March). By binning the years into cold season 1, 2, and 3, we were able to determine how many storms occurred in each cold season. Binning the storms into months allowed us to determine how many storms occurred in each month of each cold season.

To determine the frequency distribution of hurricane force extratropical cyclones in the Atlantic and Pacific basins, the cyclone position at which the first hurricane-force wind observation occurs is used. The data were placed into 5° X 5° latitude and longitude grids to create a raw frequency distribution. The raw data was subsequently smoothed by using one-eighth the sum of four times the raw central frequency plus the sum of the surrounding eight raw frequencies (Sanders and Gyakum 1980).

To determine the maximum deepening rate of each storm during its lifecycle, the Bergeron value is calculated every six hours for the preceding 24-hour time period during the cyclone's lifecycle, using the average latitude during the 24-hour period. Storms with a deepening rate greater than 1 Bergeron are classified as bombs.

2.   Composite Analyses

In conjunction with the OPC dataset, ERA-Interim metrological data from the European Center for Medium-Range Forecast (ECMWF) were incorporated to create composite analyses of relevant dynamical fields. They included temperature, vorticity, specific humidity, liquid water content, potential vorticity, and potential temperature.

To better understand the typical dynamical evolution of the hurricane-force storms, composite analyses of storms in the Atlantic and Pacific Ocean basins were created. Composites are centered on the time and location of the storm at the time it completes its maximum deepening over a 24-hour time period. We

refer to this as the '0-hour' composite. To examine the dynamical fields composited prior to and after the 0-hour composite, lag / lead composite plots were created at 6-hourly intervals subsequent / prior to the 0-hour. The composite plots were created in the following manner:

- The position at which the storm has completed 24 hours of maximum deepening is plotted on a re-gridded, relative latitude and longitude grid where the SLP center is now the (0,0) coordinate.

- The extent of the dynamic field data around the center (0,0) is a rectangular area of -40° to 40° longitude by -15° to 15° latitude.

- Summing the re-gridded dynamical field of each storm and then dividing by the number of storms creates the composite plot.

- To create anomaly composites, the monthly mean is subtracted from the data before re-gridding and summing

Composites of the temperature at 925 hPa were plotted to examine the baroclinic zone and how it evolved. Specific humidity at 925 hPa was plotted to view the moisture supply and contributor to LHR of the extratropical cyclone. Liquid water content at 925 hPa was plotted to examine the cloud structure and precipitation pattern that surrounded the cyclones. The vorticity at 500 hPa was plotted to examine the upper level support for divergence and vertical motion. The position of the eye of the vorticity vortex could give good indication of intensification or weakening of the storm. East-west vertical cross-section and horizontal (at 250 hPa) composites of potential vorticity (PV) and potential temperature (theta) at 250 hPa were plotted to examine the dynamical tropopause and upper level support for vertical motion.

3. Ensemble Prediction Data

To examine the probabilistic predictions of how high impact weather events like hurricane force extratropical cyclones by model ensemble prediction systems, data from the ECMWF and the National Center for Environmental Predictions (NCEP) model prediction systems were acquired for two randomly selected Atlantic storms from the OPC database. Tables 1 and 2 present the

OPC data for the two storms. Data was retrieved from the THORPEX Interactive Grand Global Ensemble (TIGGE) online database.

The ECMWF data has 51 ensemble members with a 0.4^o resolution, while the NCEP ensemble prediction has 21 members with a resolution of 1°. Both ensemble prediction systems have data at a 6 hour UTC intervals. These data were compared to the storm evolution in the ERA-interim.

The first storm's lifecycle is from November 27 at 1200 UTC until December 2nd at 0000 UTC. The ECMWF and NCEP ensemble prediction system used for the January storm were initialized on November 24 at 0000 UTC and the 84th hour forecast of a 144-hour forecast corresponds to November 27 at 1200 UTC, the first time-step during the examined time-steps. The time-steps highlighted in red on Table 1 are the time-steps plotted for model performance evaluation. These time steps are chosen for qualitative analysis due the dynamism of the period. During this period is when the cyclone experienced 24 hours of the most rapid deepening during its lifecycle, which occurred on November 29 at 1200 UTC.

The second storm was from January 19 at 1200 UTC until January 25th at 1200 UTC. The models were initialized on the January 16 at 1200 UTC. The 108-hour forecast of a 144-hour forecast corresponds to January 21 at 0000 UTC time-step, the first time step plotted for qualitative model performance evaluation. The cyclone ended its 24-hour of maximum deepening on January 21 at 1200 UTC.

ATL111127	2007 11 27 12	46.7	-64.0	998	G
ATL111127	2007 11 27 18	48.3	-61.7	996	G
ATL111128	2007 11 28 00	50.3	-57.7	993	S
ATL111128	2007 11 28 06	51.5	-53.4	986	S
ATL111128	2007 11 28 12	53.0	-52.5	982	S
ATL111128	2007 11 28 18	54.1	-49.8	973	S
ATL111129	2007 11 29 00	54.6	-46.4	968	S
ATL111129	2007 11 29 06	55.9	-40.7	960	S
ATL111129	2007 11 29 12	58.1	-37.5	952	H
ATL111129	2007 11 29 18	59.7	-32.2	950	H
ATL111130	2007 11 30 00	60.8	-33.9	950	H
ATL111130	2007 11 30 06	60.3	-27.9	952	H
ATL111130	2007 11 30 12	60.2	-26.6	958	H
ATL111130	2007 11 30 18	59.7	-22.3	962	H
ATL111201	2007 12 01 00	59.1	-19.8	964	S
ATL111201	2007 12 01 06	58.9	-16.2	968	S
ATL111201	2007 12 01 12	58.7	-12.3	974	S
ATL111201	2007 12 01 18	58.1	-7.9	976	G
ATL111202	2007 12 02 00	58.7	-6.1	998	G

Table 1.   November 2007 hurricane force extratropical cyclone. Starting from left to right; the first column is the storm name, second column is the year, month, day, hour (UTC), latitude, longitude, central pressure, wind threshold. Values in red indicate the 6-hour time-steps plotted on track and SLP intensification plots in Figures 69 and 70. Values in blue mark the 24th hour of maximum deepening. (After OPC data).

ATL260119	2008 01 19 12	32.5	-73.9	1014	G
ATL260119	2008 01 19 18	32.8	-73.7	1010	G
ATL260120	2008 01 20 00	36.8	-69.5	1009	G
ATL260120	2008 01 20 06	38.4	-66.1	1003	G
ATL260120	2008 01 20 12	39.7	-63.0	998	G
ATL260120	2008 01 20 18	43.5	-55.6	990	S
ATL260121	2008 01 21 00	46.3	-49.6	978	S
ATL260121	2008 01 21 06	49.4	-44.6	970	S
ATL260121	2008 01 21 12	52.4	-39.6	956	H
ATL260121	2008 01 21 18	55.6	-35.2	948	H
ATL260122	2008 01 22 00	58.2	-30.9	945	H
ATL260122	2008 01 22 06	61.7	-28.9	948	H
ATL260122	2008 01 22 12	63.8	-30.5	948	H
ATL260122	2008 01 22 18	62.3	-40.9	956	S
ATL260123	2008 01 23 00	61.5	-40.2	952	H
ATL260123	2008 01 23 06	62.4	-39.8	955	H
ATL260123	2008 01 23 12	62.4	-40.0	960	H
ATL260123	2008 01 23 18	62.9	-38.6	963	S
ATL260124	2008 01 24 00	62.9	-36.4	966	S
ATL260124	2008 01 24 06	64.0	-34.9	963	S
ATL260124	2008 01 24 12	64.2	-34.9	964	S
ATL260124	2008 01 24 18	64.7	-33.6	962	S
ATL260125	2008 01 25 00	64.8	-31.4	966	S
ATL260125	2008 01 25 06	65.0	-31.5	968	S
ATL260125	2008 01 25 12	66.1	-28.9	974	S

Table 2.   January 2008 hurricane force extratropical cyclone. Starting from left to right; the first column is the storm name, second column is the year, month, day, hour (UTC), latitude, longitude, central pressure, wind threshold. Values in red indicate the 6-hour incremental time-steps plotted on track and SLP intensification plots in Figures 71 and 72. Values in blue mark the 24th hour of maximum deepening. (After OPC data).

To plot the tracks of the ensemble members, an automated routine was designed to track the SLP minimum. At the first time period, the routine searches for the SLP minimum within a 750 km radius of the observed storm center position. For each subsequent time step (six hours later), the routine searches within a 650 km radius of the previous SLP minimum center. This process is

repeated till the end of the forecast period for each ensemble member. An example of this procedure is shown in Figure 16 for the case of ECMWF ensemble member 1 for the November 2007 storm.

The compilation of the SLP data provides both track and intensification information for each ensemble member. In addition, ensemble mean data are created.
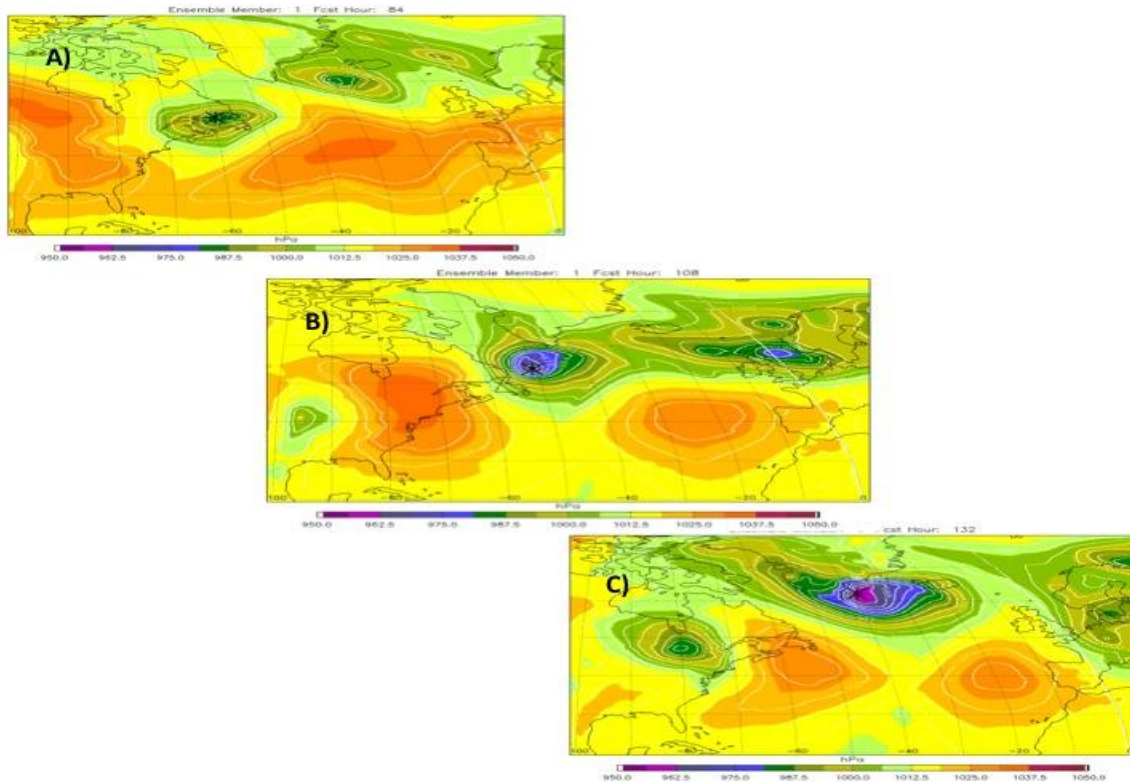
Figure 16.   Ensemble member 1 forecast. Minimum SLP marked by black asterisk. (a) 84-hour forecast for 27 November at 1200 UTC. (b) 108-hour forecast for 28 November at 1200 UTC. (c) 132-hour forecast for 29 November at 1200 UTC.

III. CLIMATOLOGY ANALYSIS

A. CLIMATOLOGY ANALYSIS

Over the cold seasons of 2006–2007, 2007–2008, 2008–2009, the Pacific and Atlantic basins experienced 124 and 135 hurricane force extratropical cyclones, respectively.
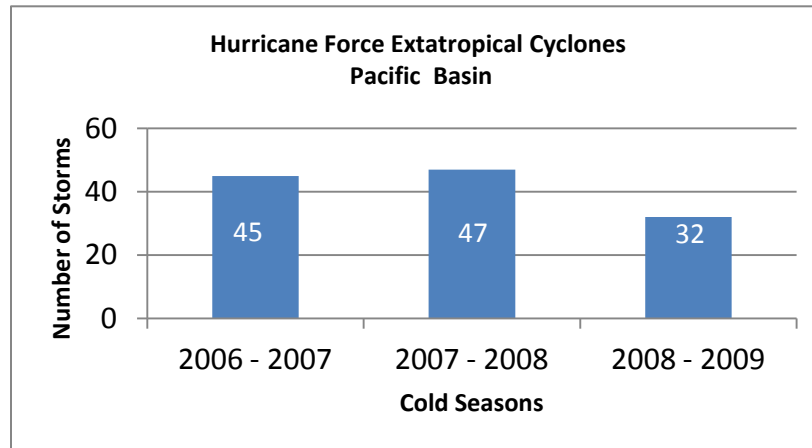
Figure 17. Total number of hurricane force extratropical cyclone in the Pacific basin during the 3 cold seasons of 2006–2009.

The distribution of storms in each cold season is shown in Figures 17 and 18. In both basins, cold seasons 2006–2007, and 2007–2008 were more active than the 2008–2009 cold season. The frequency of storms in the Atlantic and Pacific basins is qualitatively the similar.

The distribution plots of the storms by month of the Atlantic and Pacific basins are presented in Figures 19 and 20. The plots show a very similar distribution curve. In both basins, the months of December, January, and February are the most active months, as one might expect given the relative strong baroclinicity during the winter months.
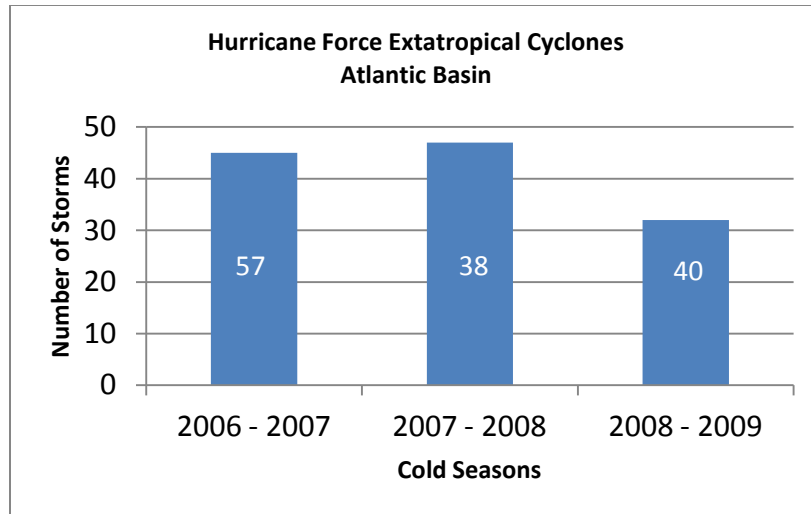
Figure 18.   Total number of hurricane force extratropical cyclone in the Atlantic basin during the 3 cold seasons of 2006–2009
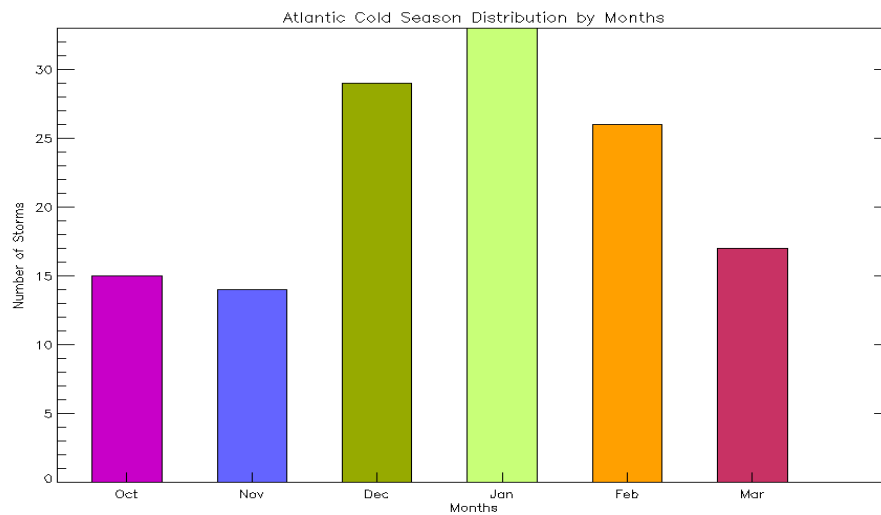
Figure 19.   Atlantic cold season distribution by months. 135 storms during cold season months of October to March 2006–2009 (left to right)
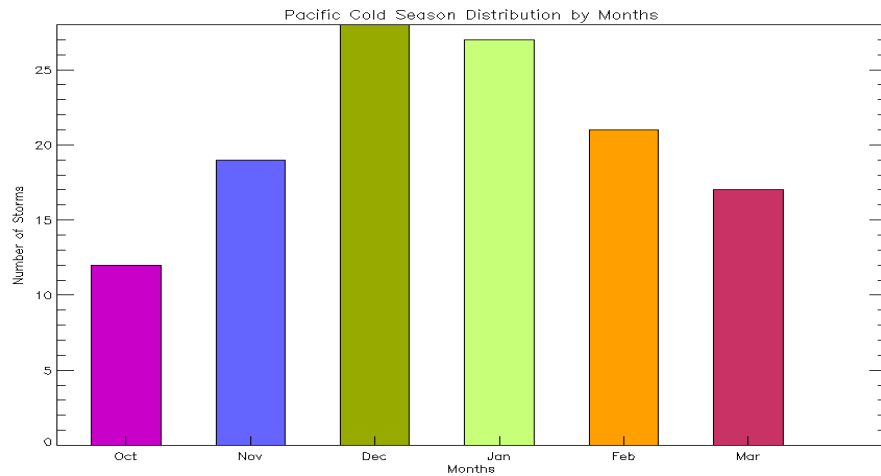
Figure 20.　Pacific cold season distribution by months.　124 storms during cold season months of October to March 2006–2009 (left to right)
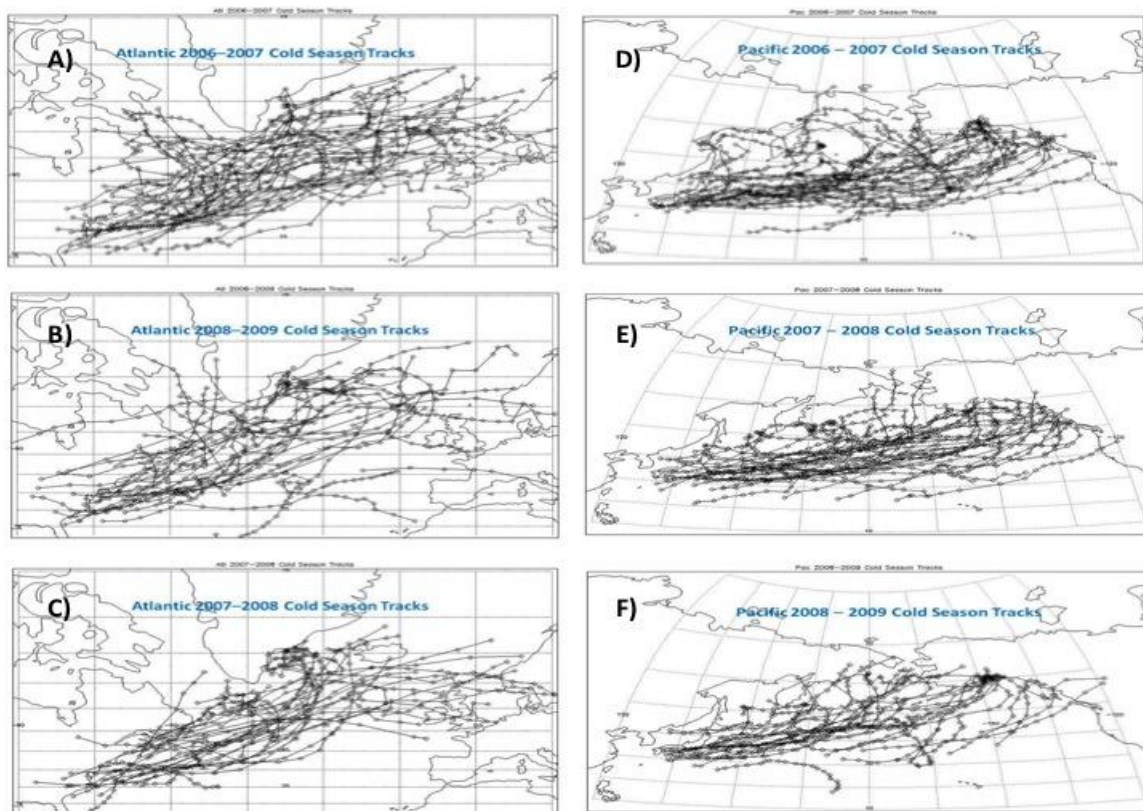
Figure 21.　Atlantic and Pacific cold season storm tracks.　(a) Atlantic 2006–2007. (b) Atlantic 2007–2008. (c) Atlantic 2008–2009. (d) Pacific 2006–2007. (e) Pacific 2007–2008. (f) Pacific 2008–2009

31
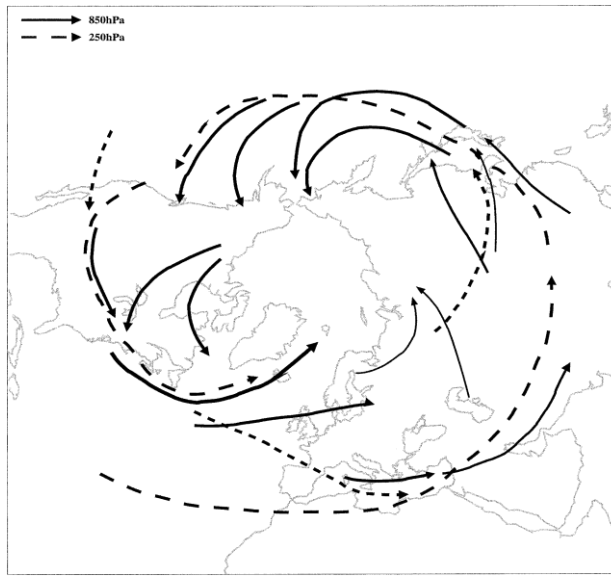
Figure 22. Schematic of principal tracks for lower—(solid line) and upper—
(dashed line) tropospheric storm track activity based on relative
vorticity at 850 hPa and theta at the PVU 2 surface. (From Hoskins
and Hodges (2002))

Using the latitude and longitude of the cyclones from the OPS dataset to plot storm tracks of all of the cold season storms in the Atlantic and Pacific basin, revealed results consistent with previous studies on storm tracks, cyclogenesis, and cyclolysis by Hoskins and Hodges (2002) who conducted a study on northern hemisphere winter storm tracks. The primary data used by Hoskins and Hodges (2002) for their study were 6-hourly data for the 22-yr period 1979–2000 (from the 15-yr ECMWF Reanalysis). They identified areas of cyclogenesis around the world to be baroclinic zones, including off the east coast of the United States and to the east of Japan, in good agreement with the results herein. Using mean sea-level pressure and 850 hPa vorticity for lower level tracking, and the dynamic tropopause for upper level tracking, Hoskins and Hodges (2002) created a summary plot for global extratropical cyclone tracks (Figure 22). Figure 27 shows the general path of extratropical cyclones and Hoskins and Hodges (2002) results are consistent with our results plotted in Figures 21, despite the different dataset and methodology used to track the cyclones.

Despite the fact that the OPC database does not include information before or after the wind thresholds are surpassed, plots of the storm position at the first observation (Figure 23) and the last observation (Figure 24), are consistent with previous studies on the locations of cyclogenesis and cyclolysis, respectively. The green dots, which denote the positions of the storms once the maximum wind become greater than 34 kts, are concentrated in areas of enhanced baroclinicity previously identified. The red dots denote the position of the storm once the maximum wind goes below 34 kts. Unlike the green dots, the red dots are spread out across the ocean along the general path of extratropical cyclones, except for in the Pacific where there is a concentration of red dots in the Gulf of Alaska. This observation agrees with Hoskins and Hodges (2002) findings. They conclude that cyclolysis occurs throughout the storm track region, as well as relatively confined regions such as the Gulf of Alaska, and Vancouver region, north eastern Canada, eastern Mediterranean and central Russia.

Wernli and Schwierz (2006) created climatology of extratropical cyclones using a method by which a cyclone is identified as a finite area that surrounds a local SLP minimum and is enclosed by the outermost closed SLP shows results similar to our findings. By applying this method to individual time instants, cyclone frequencies are found by taking time averages. They applied their method to a global SLP dataset that encompasses data from 1958–2001 from the European Center for Medium-Range Weather Forecast (ECMWF) Re-Analysis (ERA-40).

According to Wernli and Schwierz (2006) during the winter months, cyclogenesis is most frequent in the following locations:

- Western Pacific in the Japan sea, southwest of Japan, and east of Japan (30°–40° N)

- Western Atlantic along the U.S east coast form South Carolina to Massachusetts (32°–41° N)

These areas are conducive to cyclogenesis due to the warm currents of the Gulf Stream and the Kuroshio Current, which enhance baroclinic instability.

33

Figures 23 and 24 from our study agree with Wernli and Schwierz (2006) findings.
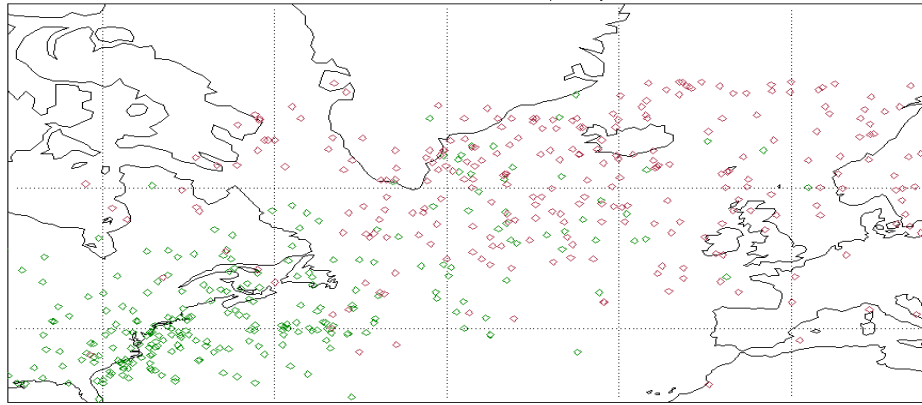
Figure 23.　Atlantic basin. Green diamonds denote position of when hurricane force wind extratropical cyclone wind speeds become greater than 43-knot (L) winds speed threshold. Red diamonds denote where storms winds speed become lower than 43 knots.
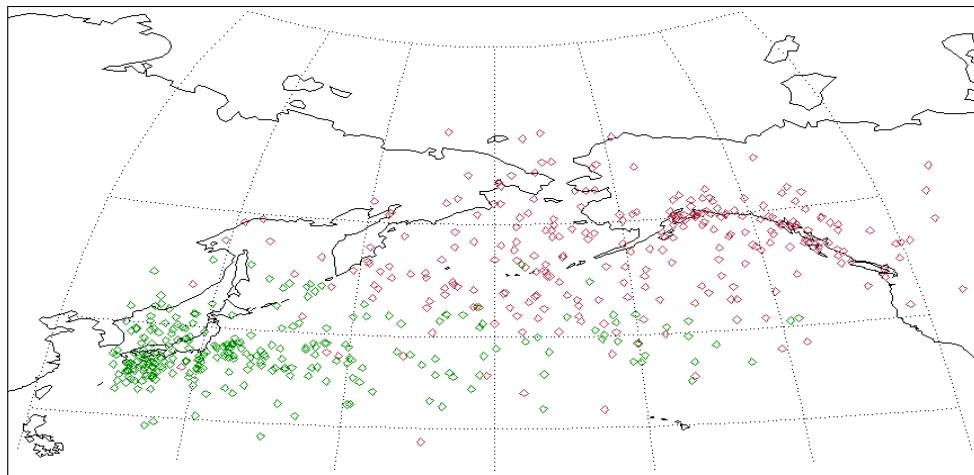
Figure 24.　Pacific basin. Green diamonds denote position of when hurricane force wind extratropical cyclone wind speeds become greater than 43-knot (L) winds speed threshold. Red diamonds denote position

The hurricane force extratropical cyclone frequency plots of the Atlantic and Pacific basins in Figure 25 and 27 are similar to the climatology of cyclones by Wernli and Schwierz (2006), despite the difference in cyclone identification method/classification, and dataset. Wernli and Schwierz (2006) plot frequency

distribution of cyclones in quarters. The results during the months of December, January, and February (DJF) are most applicable to our study since as our results show, those are the most active months for hurricane force extratropical cyclones. The DJF cyclone frequency plot from Wernli and Schwierz (2006) is shown in Figure 26.

Wernli and Schwierz (2006) show their maximum number of cyclones in the Atlantic to occur to the south east of Greenland. Our climatology shows a maximum in this area also. In the Pacific Wernli and Schwierz's (2006) maximum area is east of Japan, and our climatology is once again in accord with Wernli and Schwierz (2006). The hurricane-force climatology does exhibit two maxima in the Pacific. This is likely the result of the relatively small sample size.
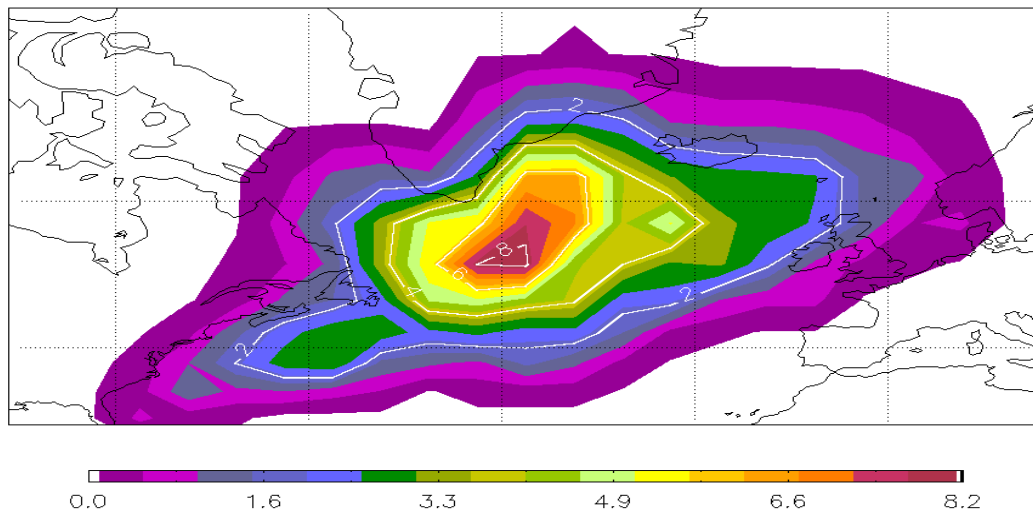
Figure 25.   Distribution of hurricane force wind extratropical cyclones in the Atlantic during the 2006–2007, 2007–2008, and 2008–2009, cold seasons. Raw non-zero frequencies appear in each 5° x 5° quadrilateral of latitude and longitude. Isopleths represent smoothed frequencies, obtained as one-eighth of the sum of four times the raw central frequency plus the sum of the surrounding raw frequencies
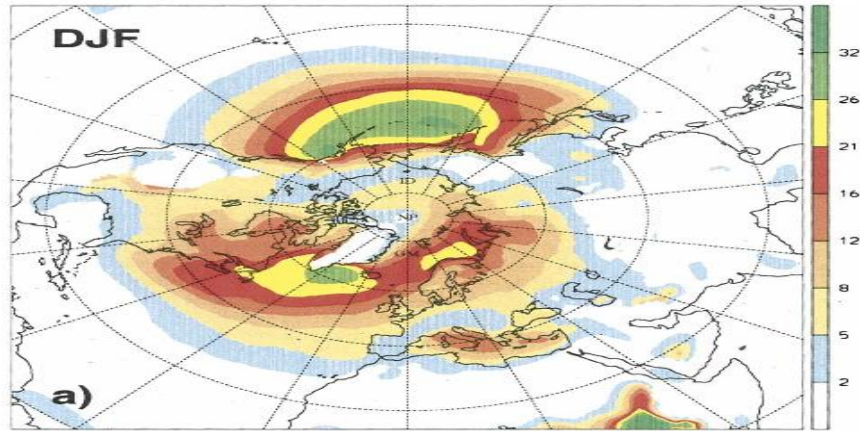
Figure 26.   Seasonal mean cyclone frequency plot Cyclone (From Wernli and Schwierz (2006)).
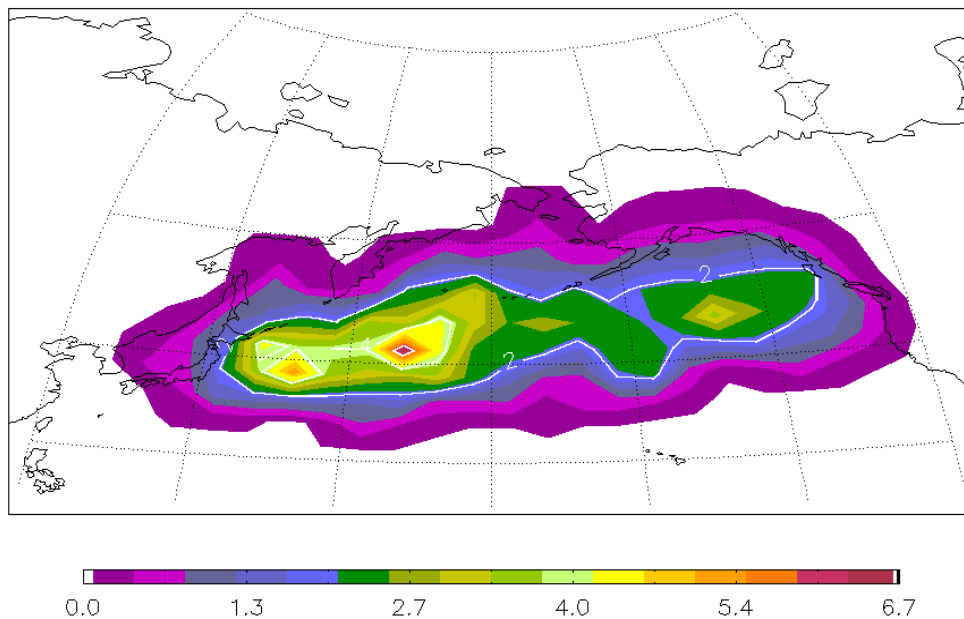
Figure 27.   Distribution of hurricane force wind extratropical cyclones in the Pacific during the 2006–2007, 2007–2008, and 2008–2009, cold seasons. Raw non-zero frequencies appear in each 5° x 5° quadrilateral of latitude and longitude. Isopleths represent smoothed frequencies, obtained as one- eighth of the sum of four times the raw central frequency plus the sum of the surrounding raw frequencies.

The average minimum SLP attained in the Pacific is 966.5 hPa. While in the Atlantic, the average is 961.7mb. Figure 28 displays the combined minimum SLP distribution in the Atlantic basin during the colds season of 2006–2009, while Figure 29 shows the Pacific basin. The SLP alone does not say much about the intensity of the storm without knowing the latitude position. The average latitude of the cyclones in the Atlantic was 59.7 degrees and in the Pacific 54.16 degrees. The average latitude and minimum SLP values were relatively close despite the Atlantic basin having a broader SLP range (928 hPa–994 hPa) versus the Pacific basin (940 hPa–995 hPa).
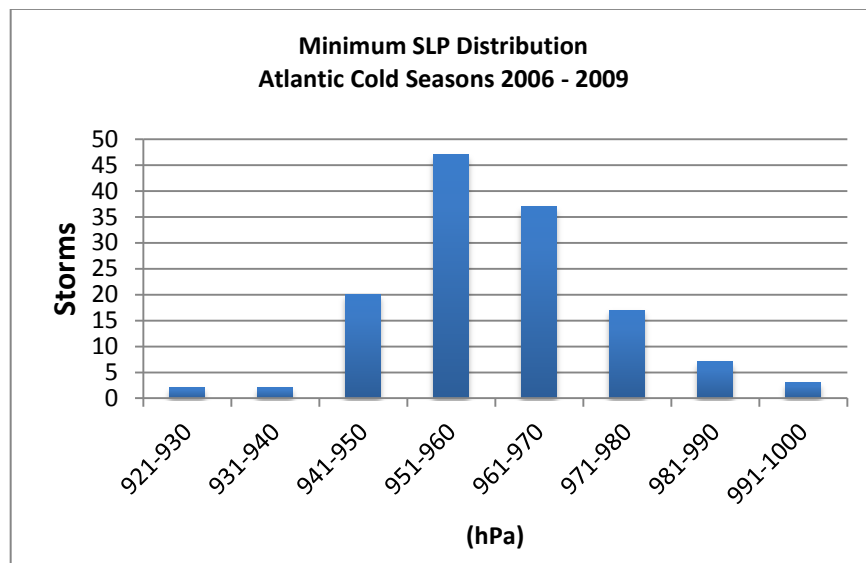
Figure 28.   Combined minimum SLP Atlantic cold season 2006–2009
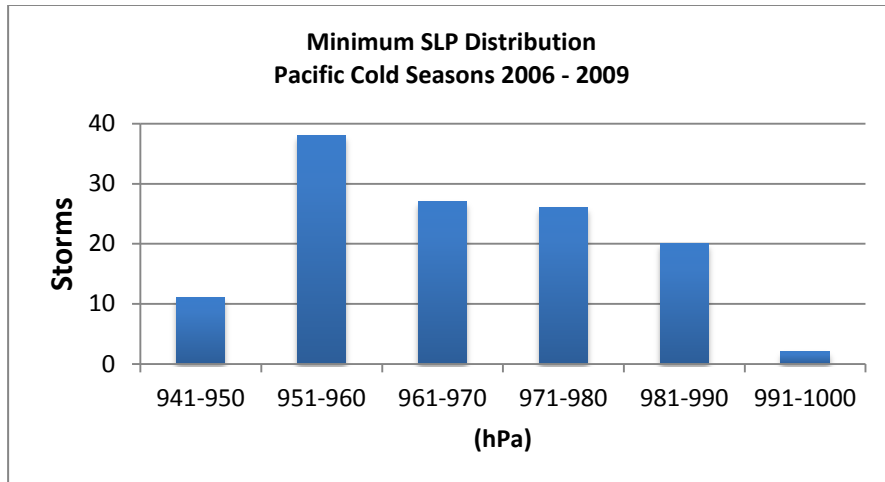
Figure 29.   Combined minimum SLP Pacific cold season 2006–2009

Hurricane force wind longevity in the Atlantic and Pacific basins during the three cold seasons proved to be similar as well (see Figure 30). The average duration of hurricane force winds in the Atlantic basin was 22.4 hours, slightly higher than in the Pacific basin where the average duration is 19.6 hours.
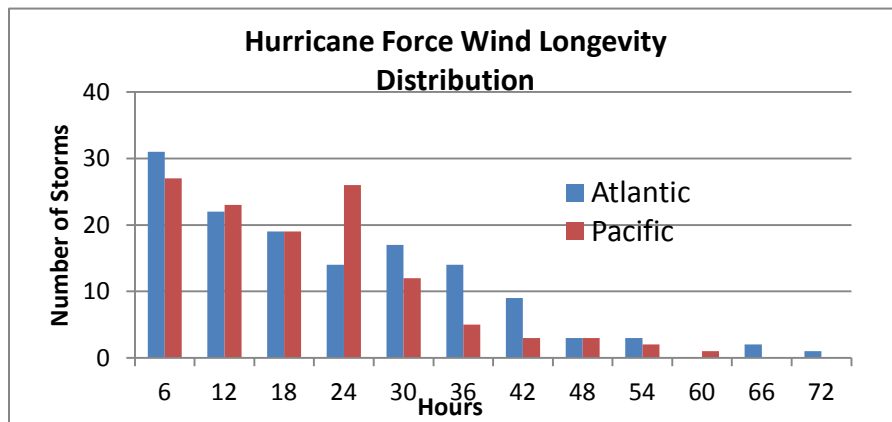
Figure 30.   Hurricane-force wind distribution in 6-hour increments during cold season 2006–2009. Blue bars represent the Atlantic basin. Red bars represent the Pacific.

Using data from the National Meteorological Center (NMC) from the periods of 2 October 1976–30 March 1977, 10 September 1977–31 March 1978, and 9 September 1978–13 April 1979, Sanders and Gyakum (1980) compared the 1200 GMT central pressures of a low on successive days to obtain the raw

deepening, and calculate the Bergeron value to determine if a storm deepened explosively (bombed). During the three-year period, 267 of the storms in the Atlantic and Pacific basins were classified as bombs (the frequency distribution is shown in Figure 7).

Comparing the results from the hurricane force frequency distribution plots in Figures 25 and 27 to the results in Figure 7 from Sanders and Gyakum (1980), reveals a strong similarity in hurricane force extratropical cyclones and extratropical cyclone that bomb. Sanders and Gyakum (1980) show that bombs are primarily maritime events, consistent with the results here. Figure 7 also shows maximums in areas of the Atlantic and Pacific that are qualitatively similar to the results in Figures 25 and 27.

The similarity in results despite Sanders and Gyakum's consideration of storms that bombed stems from the fact that majority of the hurricane force extratropical cyclones exhibited explosive deepening. Figures 31 and 32, displays the number of bombs in comparison to total number of storms during the cold seasons of 2006–2009 in the Atlantic and Pacific basins.
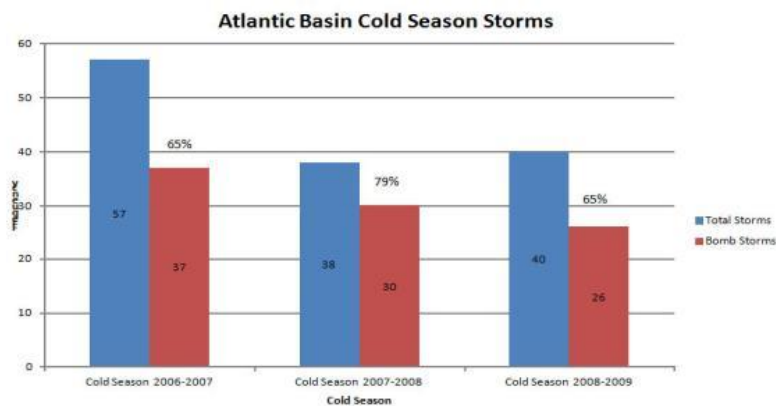
Figure 31.   Atlantic cold season 2006–2009. Blue bar is the total number of storms per season. Red bar represents the number of storms within the season that experienced deepening rate greater than 1 Bergeron.
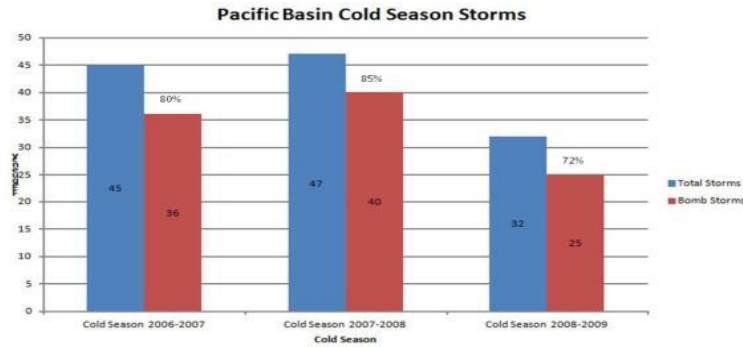
Figure 32. Pacific cold season 2006–2009. Blue bar is the total number of storms per season. Red bar represents the number of storms within the season that experienced deepening rate greater than 1 Bergeron.

Of the 259-hurricane force extratropical cyclone catalogued during the cold seasons of 2006–2009 in the Atlantic and Pacific basins, 194 (75%) were qualified as bombs (i.e. had a maximum deepening rate greater than one Bergeron) The Pacific basin exhibited a higher percentage of bombs than the Atlantic basin, as Figures 31 and 32 demonstrate. Of the 124 Pacific storms, 79% were bombs. In comparison, 70% of 135 Atlantic Storms explosively deepened

Figures 33 and 34 are frequency distribution plots of the position at which the extratropical cyclones experienced their maximum deepening rate (24-hours of deepening, bomb or no bomb) in the Atlantic and Pacific basin. The plots bear a strong qualitative resemblance to the overall storm frequency data (Figures 25 and 27). Comparison of these plots gives further evidence of significant similarity between explosive deepening and hurricane force extratropical cyclones.
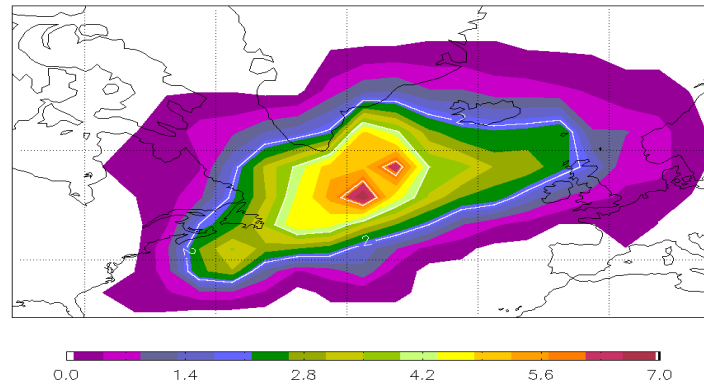
Figure 33.   Frequency distribution of cyclones at 24 hours of maximum rapid
deepening during lifecycle in the Atlantic basin during cold seasons
2006–2009
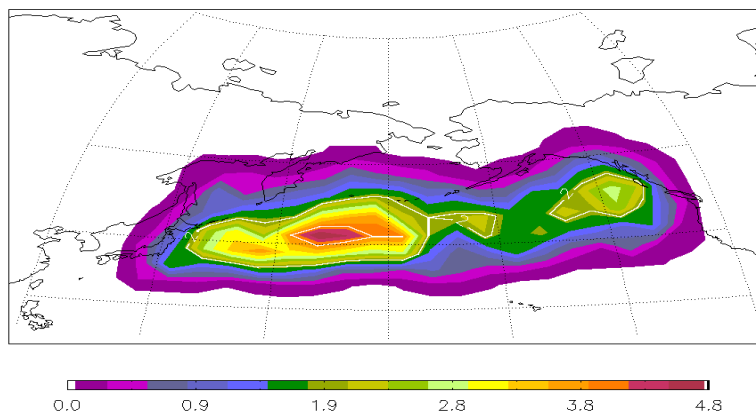
Figure 34.   Frequency distribution of cyclones at 24 hours of maximum rapid
deepening during lifecycle in the Pacific basin during cold seasons
2006–2009

When calculating and plotting the maximum deepening rate distribution of
the storms in the Atlantic and Pacific basins, a few of the storms cyclones show a
deepening rate of zero. Examining the data reveals that these storms show an
increase in pressure during the duration from when the wind of the extratropical
cyclone increase above the L wind threshold, and the OPC database began
tracking storm.   This is very unlikely and is possible that the extratropical
cyclones may have experienced explosive deepening before the winds reached

41

the L threshold. In light of this, as stated above, it is likely that more of the hurricane force wind extratropical cyclones experienced explosive deepening above the 70% and 79% values for the Atlantic and Pacific basins, respectively.

Figure 35 and 36 display the deepening rate distribution of the Atlantic and Pacific basin during the cold season of 2006–2009. A 0.1 Bergeron bin is used to bin the deepening rates of the storms. Roebber (1984), in his statistical analysis and updated climatology of explosive cyclones, produced a similar plot (see Figure 37) in which he shows the 24-hour deepening rate distribution of all extratropical cyclones between February of 1980 and January of 1981. There is a significant overlap between storms that bomb and hurricane force storms. Again, this highlights the fact that the vast majority of hurricane force storms undergo explosive deepening.
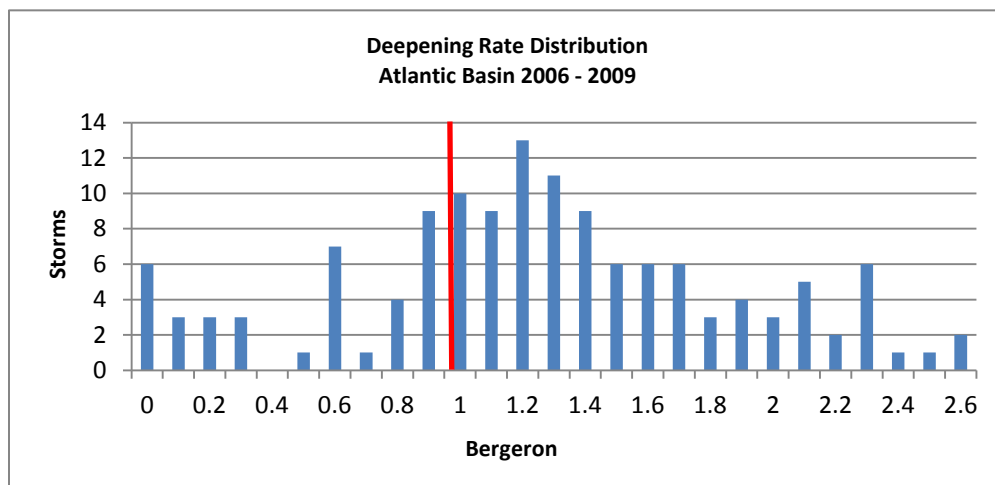
Figure 35.   Combined deepening rate distribution of the Atlantic basin cold seasons form 2006–2009. All storms to the right of the red line are considered bombs.
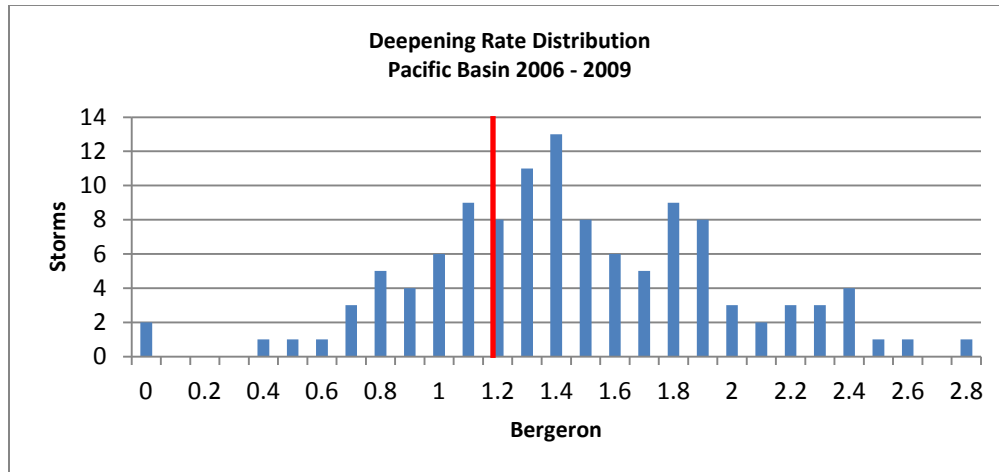
Figure 36.   Combined deepening rate distribution of the Pacific basin cold
             seasons form 2006–2009. All storms to the right of the red line are
             considered bombs.
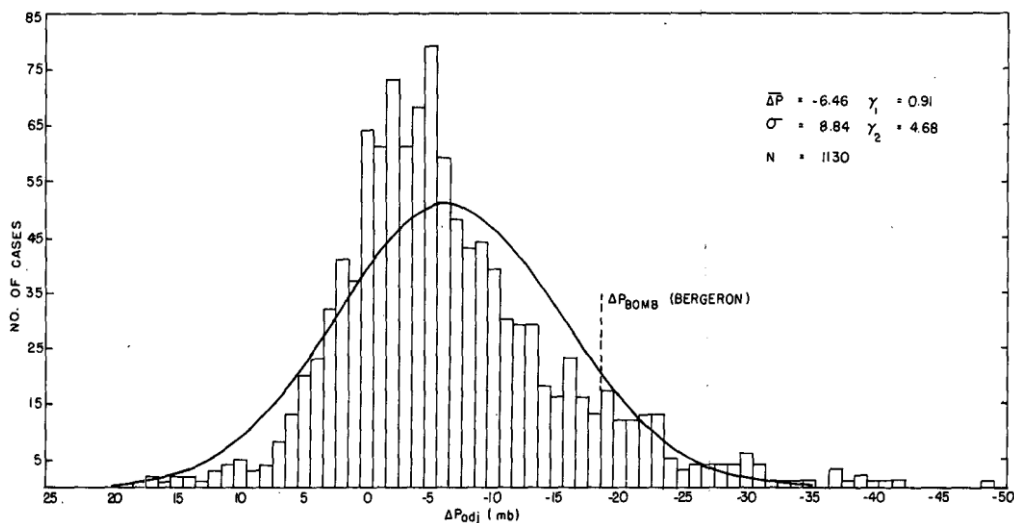
Figure 37.   From Roebber (1984). 24-hour deepening rate distribution, one-year
             data. The dashed line indicates the Bergeron definition of a bomb;
             points to the right of the line are bombs.

Presented in Figure 38 and 39 is the bomb distribution by month for the Atlantic and Pacific basins for the cold seasons of 2006–2009. Figures 41, 42, and the associated tables, present the deepening rate distribution by months and percentage breakdowns. To prevent skewing of the results, we have removed the storms that had Bergeron values of 0.0–0.50, as these values are likely not

representative of the actual storm deepening rate. Figures 38–41 show that the months of December, January and February are the most active months for hurricane force wind extratropical cyclones in both the Atlantic and Pacific basins. In the Atlantic, 63% of all of the hurricane force storms occurred during those 3 months, while the Pacific basin experienced 62% of its storms during those months. The most intense storms with Bergeron values greater than 2 only occur during the months of December, January and February. Figure 42 adapted from Sander and Gyakum (1980) is in accord with these results.
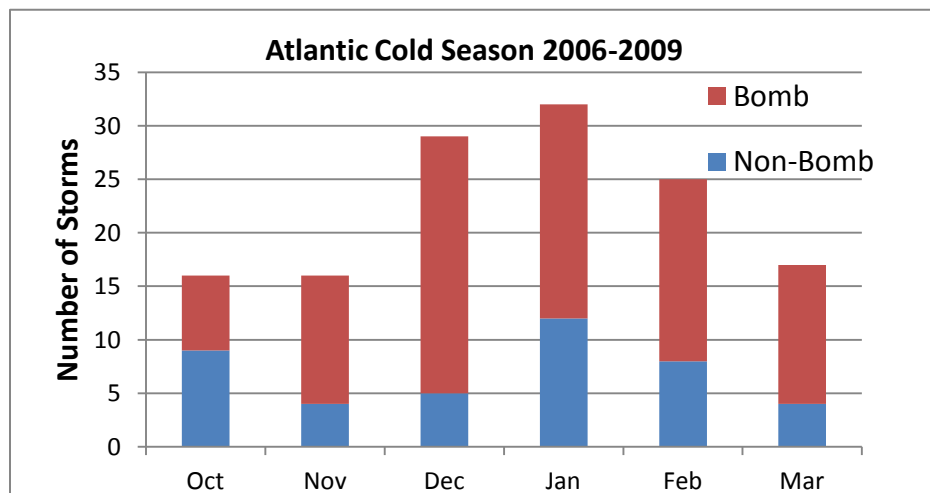
Figure 38.　Atlantic cold season 2006–2009 bomb distribution by month. Red represents bombs and the blue represent non-bombs. The combination of the red and blue bar yields the total number of storms.
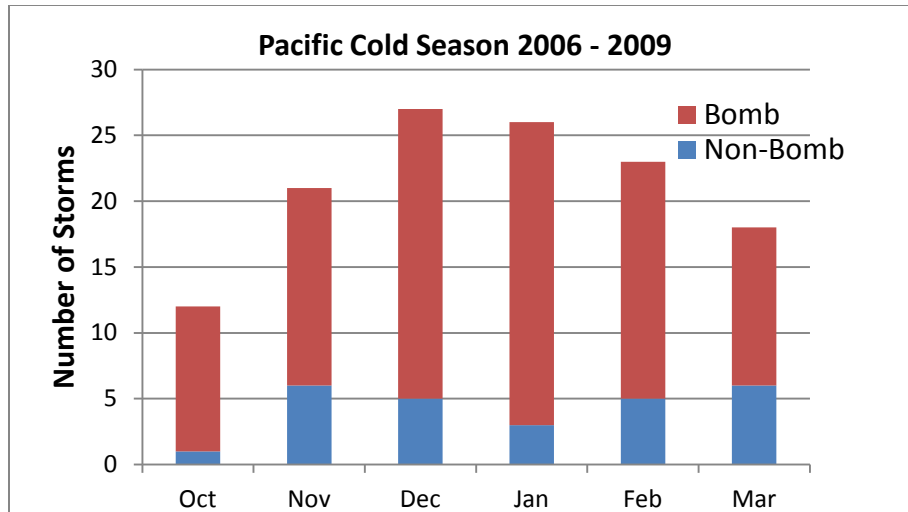
Figure 39. Pacific cold season 2006–2009 bomb distribution by month. Red represents bombs and the blue represent non-bombs. The combination of the red and blue bar yields the total number of storms.
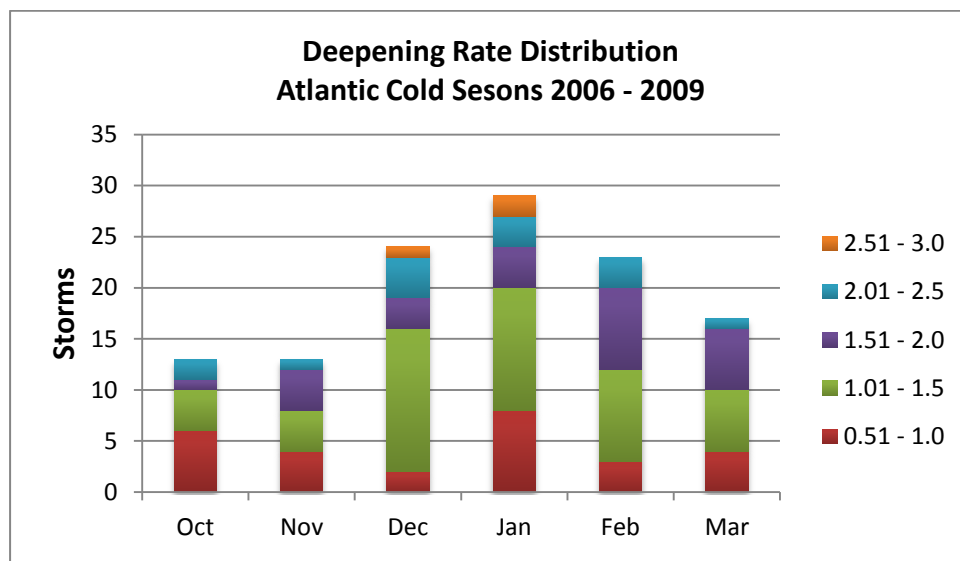
Figure 40. Atlantic deepening rate distribution by months for the cold season of 2006–2009. The legend indicates Bergeron values in 0.5 incremental bins.

	Deepening Rate (Bergeron)						
	0.51–1.0	1.01–1.5	1.51–2.0	2.01–2.5	2.51–3.0		
Oct	46%	31%	8%	15%	0%	**11%**	
Nov	31%	31%	31%	8%	0%	**11%**	
Dec	8%	58%	13%	17%	4%	**20%**	**Total %**
Jan	28%	41%	14%	10%	7%	**24%**	**(Months)**
Feb	13%	39%	35%	13%	0%	**19%**	
Mar	24%	35%	35%	6%	0%	**14%**	
Total %	**25%**	**39%**	**22%**	**12%**	**2%**		

Table 3.   Atlantic 2006–2009 cold season deepening-rate distribution percentage breakdown. The bold numbers at the bottom of the table represent the percentage of storms in each 0.5 incremental Bergeron bin. The bold numbers to the side represent the percentage of storms in each month.
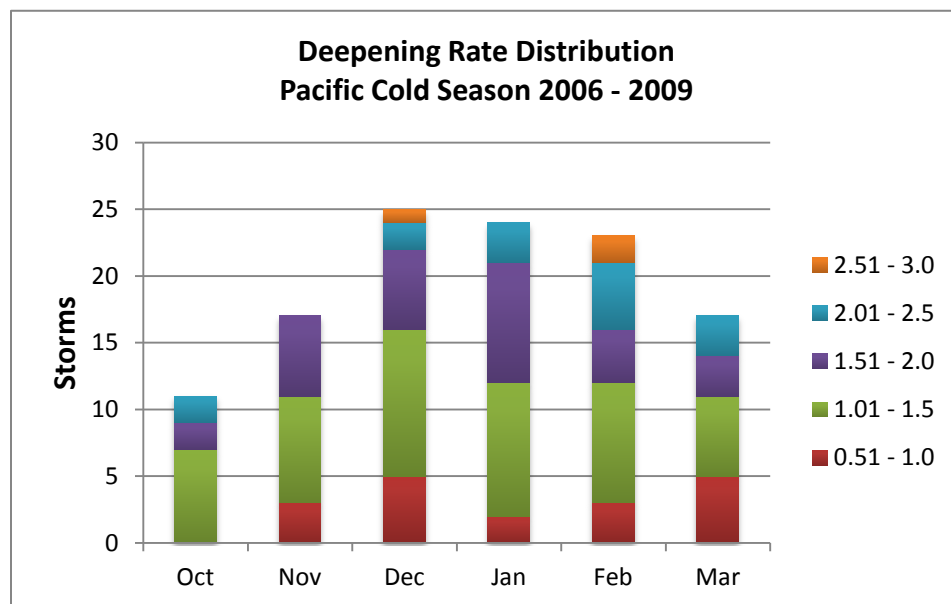
Figure 41.   Pacific deepening rate distribution by months for the cold season of 2006–2009. The legend indicates Bergeron values in 0.5 incremental bins.

	Deepening Rate (Bergeron)						
	0.51–1.0	1.01–1.5	1.51–2.0	2.01–2.5	2.51–3.0		
Oct	0%	64%	18%	18%	0%	**9%**	
Nov	18%	47%	35%	0%	0%	**15%**	
Dec	20%	44%	24%	8%	4%	**21%**	**Total %**
Jan	8%	42%	38%	13%	0%	**21%**	**(Months)**
Feb	13%	39%	17%	22%	9%	**20%**	
Mar	29%	35%	18%	18%	0%	**15%**	
Total %	**15%**	**45%**	**25%**	**13%**	**2%**		

Table 4.   Pacific 2006–2009 cold season deepening-rate distribution percentage breakdown. The bold numbers at the bottom of the table represent the percentage of storms in each 0.5 incremental Bergeron bin. The bold numbers to the side represent the percentage of storms in each month.
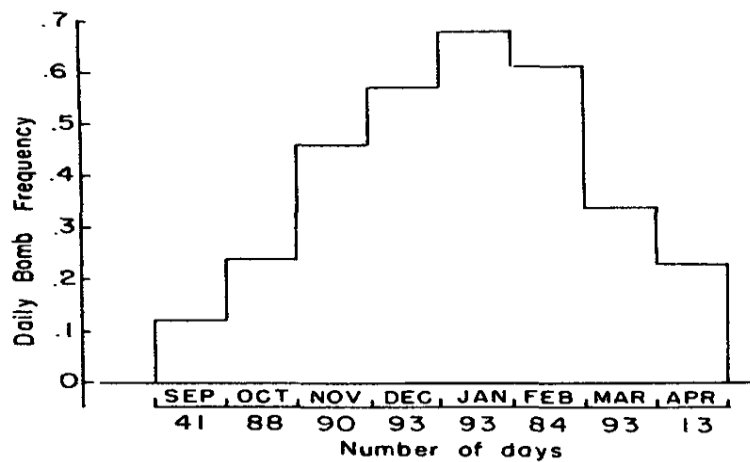
Figure 42.   Mean daily bomb frequency as a function of calendar month, for the three cold seasons in their study. The abscissa indicates the number of days considered for each. (From Sanders and Gyakum (1980)).

THIS PAGE INTENTIONALLY LEFT BLANK

IV.   COMPOSITE ANALYSIS

In an effort to better understand the dynamical evolution of hurricane-force extratropical cyclones, the composite structure of relevant meteorological variables were created.   The composites center on the time, and position at which the hurricane-force extratropical cyclones have just completed 24-hours of maximum deepening rate during their lifecycle as recorded in our OPC dataset.

In a fashion similar to Rogers and Bosart (1986), to examine the structure of the hurricane-force extratropical cyclones, we will employ a four-fold, temporal process.   Firstly, the 0-hour composite of the dynamical fields described earlier in the methodology section will be examined to discuss the structure of the storms at the onset of the mature stage as defined by Rogers and Bosart (1985). Secondly, the anomalies of the dynamical fields at the 0-hour will be examined to qualitatively examine the anomalous nature of the dynamic fields.   Thirdly, a look back in time at anomaly composites will be used to give a sense of storm evolution, and environmental conduciveness to cyclogenesis during the incipient and explosive stages.   Lastly, a look forward in time from the 0-hour composite can give a peak into the cyclolysis stage, and assist in determining what conditions contribute to the decay of the hurricane force extratropical cyclones. Except for instances where there are notable dissimilarities worth mentioning, we use the composites of the Atlantic basin in this section (as the results from the Atlantic and Pacific basins are qualitatively similar).

A.   0-HOUR COMPOSITES (MATURE STAGE)

The 0-hour composite occurs at the end of the 24-hour period of time that exhibited the maximum deepening rate.   This corresponds to the end of the explosive stage and the onset of the mature stage as defined by Rogers and Bosart (1985).   Rogers and Bosart's (1985) definition of the mature stage is that the rapid central pressure falls ceases to occur and the central pressure, strength, and areal extent of the cyclone's circulation remain steady.   In some of

the hurricane force extratropical cyclones in the OPC dataset, the pressure attained during the 24-hour period of rapid pressure fall is the minimum SLP attained during the storm lifecycle. After the 24-hours of maximum rapid deepening, the average delay before the SLP minimum began to rise is approximately six hours. This agrees well with Rogers and Bosart's definition of the mature stage. We use the term 'explosive stage' loosely. Unlike Rogers and Bosart (1985), where all the storms in their composite study bombed according to the > 12 hPa $(12h)^{-1}$ criteria, only 75% of the hurricane force extratropical cyclones bombed in our study in accordance with the geostrophically adjusted 1 hPa h^{-1} for 24 hours at 60° latitude criteria.

The composite of the temperature field at 925 hPa with SLP overlaid is presented in Figure 43. That there is a significant baroclinic zone is apparent. In addition, the cyclonic rotation of the storm has caused the temperature contours in the baroclinic zone to deform.
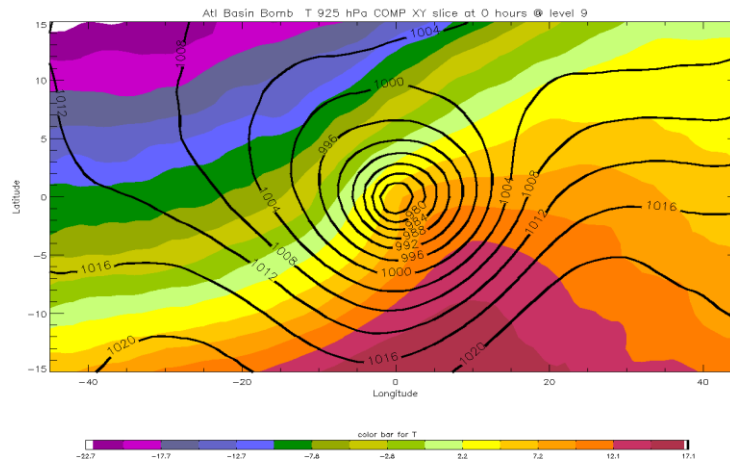
Figure 43.   0-hour composite of 135 storms in the Atlantic basin from the cold
season of 2006–2009. Colors are the temperature field at 925 hPa
ranging from -22.7–17.1 degrees Celsius. Black lines are SLP
contours (intervals of 4 hPa).

Warmer (colder) relative temperatures are found to the east (west) of the storm center. This pattern is the result of the warm and cold air advection taking place. The warm and cold air advection at lower levels serves to help build the

ridge and trough aloft. The cyclonic flow of air around the trough axis is where positive vorticity is at a maximum. Figure 44 displays the vorticity field at 500 hPa with SLP overlays. The SLP minimum and the vorticity maximum are almost vertically stacked at the 0-hour. However, there is still a slight tilt to the southwest. Martin (2006) explains that purely vertical stacking results in the displacement of the upper divergence maximum to the east of the sea level pressure minimum. This displacement of the upper level divergence reduces air mass evacuation aloft over the surface pressure low, causing the surface pressure tendency to become positive. In association with the decrease in surface pressure, there will be reduced cold and warm temperature advection. The displacement of the upper level divergence disrupts the positive feedback loop that an extratropical cyclone needs for intensification and growth. The slight tilt to the southwest at the 0-hour in our composite explains why there is an average continued slow fall of pressure for about 6 hours until minimum SLP is obtained. The reduction and eventual absence of vertical motion is necessary for the storm to move into the decay stage.
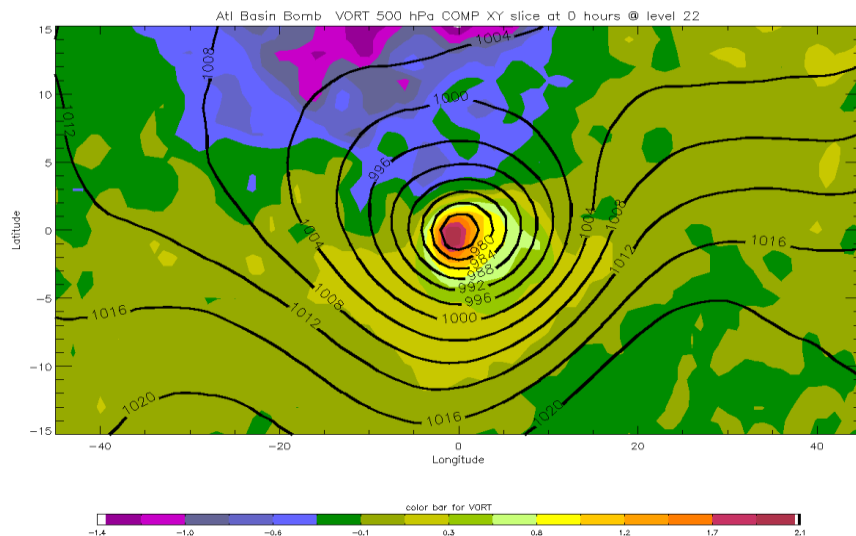
Figure 44. 0-hour composite of 135 storms in the Atlantic basin from the cold season of 2006–2009. Colors are for the vorticity field at 500 hPa ranging from -1.4 to 2.1. Black lines are SLP contours (intervals of 4 hPa).

The west-east vertical cross section of the composite PV and potential temperature (θ) at the 0-hour is presented in Figure 45. These data provide further evidence of the vertical stacking of the system: the 'PV tower' shows little to no tilt with height. At upper-levels, the positive / negative PV anomaly couplet is observed. It is hypothesize here that diabatic processes have contributed significantly to the downstream ridge
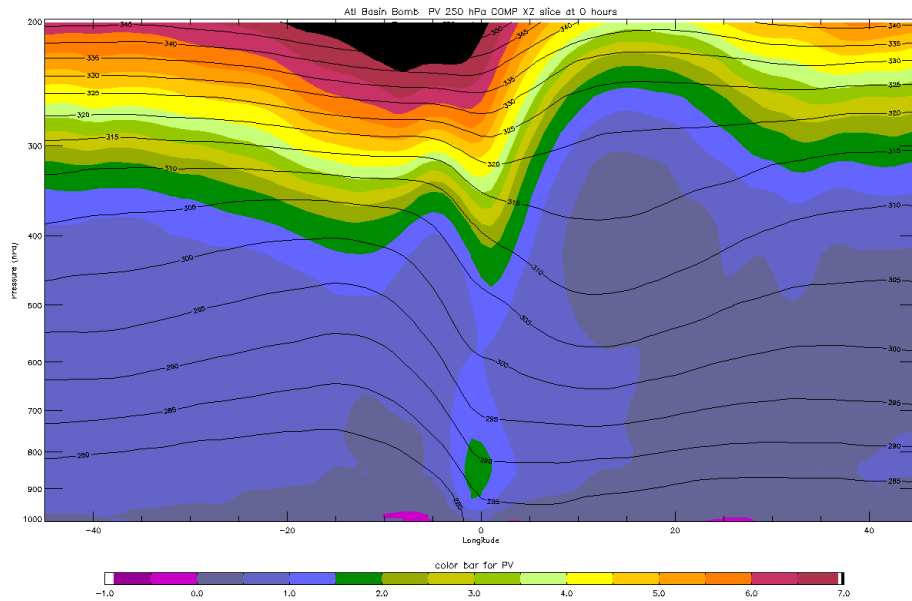
Figure 45.   Atlantic basin vertical cross section composite at the 0-hour of potential vorticity (PV) (colored contours) and Theta (θ) (black lines intervals of 5 K). Cross section is from 1000 hPa to 200 hPa. Green contour is 2 PVU, approximately tropopause level.

Composite of the total wind at 250 hPa at the 0-hour captures the shortwave trough within the jet stream that enhances upward vertical motion depending on the location relative to the surface low and aids in intensifying an extratropical cyclone. In Figure 46, the winds decrease to the left and right of the velocity field center. That means that air coming from the west of the velocity center is converging, while to the east the air is diverging. Due to the cyclone being in a mature stage, the center of the jet streak is directly above the surface low and the upper-level divergence is not serving to intensify the cyclones.
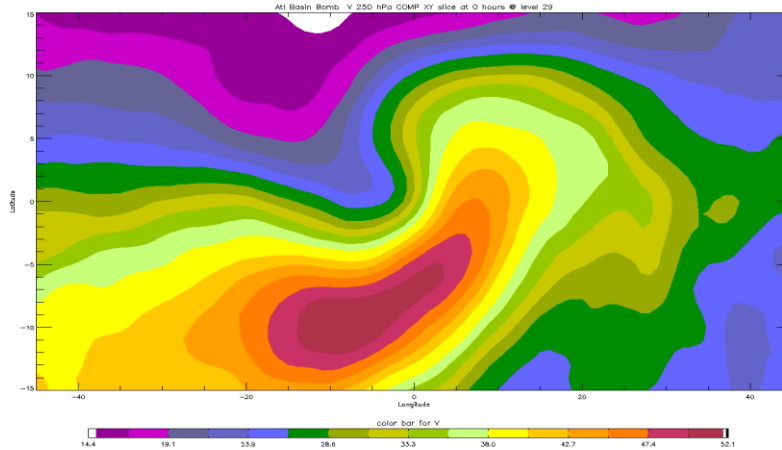
Figure 46.   Atlantic composite at the 0-hour of wind velocity field at 250 hPa. Colors are the wind speed contours and they range from 14.4 ms^{-1} to 52.1 ms^{-1}.

B.   0-HOUR ANOMALY COMPOSITES

The anomaly composites, which are the composited difference between the re-gridded data and the monthly mean, give a qualitative measure of how unusual from the norm a dynamical feature may be. The anomaly composite of temperature at 925 hPa at the 0-hour (Figure 47) shows the cumulative effect of the low-level temperature advection associated with the storms.

While there appears to be a considerable amount of anomalous cyclonic vorticity (Figure 48), the upper level trough axis is in a vertically stacked position relative to the surface low-pressure center, displacing maximum divergence to the east of the low-pressure center. This indicates the cyclone is at the onset of weakening.

Figure 49 represents a west-east vertical cross-sectional anomaly plot of PV from 1000 hPa to 200 hPa. The plot illustrates that positive low-level and upper-level PV anomalies are nearly vertically stacked. The anomalies appear to be phase locked, or are interacting with one another. As with, the surface low and the upper level trough, a westward tilt with height between the surface and upper level PV anomalies is needed for an intensifying cyclone.   The nearly

53

vertically stacked nature of the PV anomalies in Figure 49 indicates the intensity of the storm is subsiding at the 0-hour composite.

Figure 49 also shows a significant negative PV anomaly aloft. Diabatic heating contributes to this negative PV anomaly. Lifted air rises most vigorously downstream of the upper-level positive PV anomaly. As the air rises, the release of latent heat builds the ridge downstream of the positive PV anomaly trough. The amplification of the ridge shortens the wavelength between the upper level trough and downstream ridge. This increase in slope between the PV anomalies makes the PV anomaly more anomalous as shown in Figure 52, Martin (2006). The more anomalous, the more intense the cyclone will become, hence the positive feedback loop. Figure 45 most clearly displays the downstream PV anomaly ridge. This process of building the downstream ridge of a positive PV anomaly is an example of how diabatic heating serves an as energy source for extratropical cyclones.

The warm moist supply of air for latent heat release comes is predominantly associated with the warm conveyor belt. This is true and is evident in the anomaly composite of specific humidity at the 0-hour at 925 hPa (Figure 50). Figure 51 shows the liquid water content anomaly composite at the 0-hour at 925 hPa. The liquid water content plot resembles the cloud pattern associated with extratropical cyclone when viewed from a satellite and agrees with previous studies on the typical shape of the cloud pattern. In order to have cloud formation, condensation must have occurred and latent heat released. Latent heat, from all indications, is an important secondary energy source for the intensification of hurricane force extratropical cyclones.
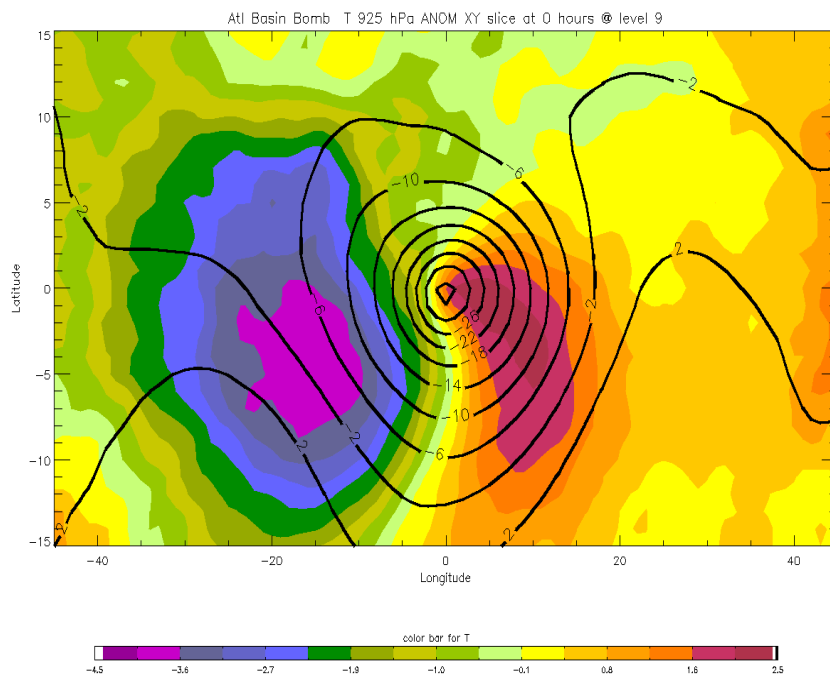
Figure 47.   0-hour anomaly composite of Atlantic temperature field at 925 hPa.
Colors range from -4.5–2.5 degrees Celsius. Black lines are SLP
anomaly contours (intervals of 4 hPa).
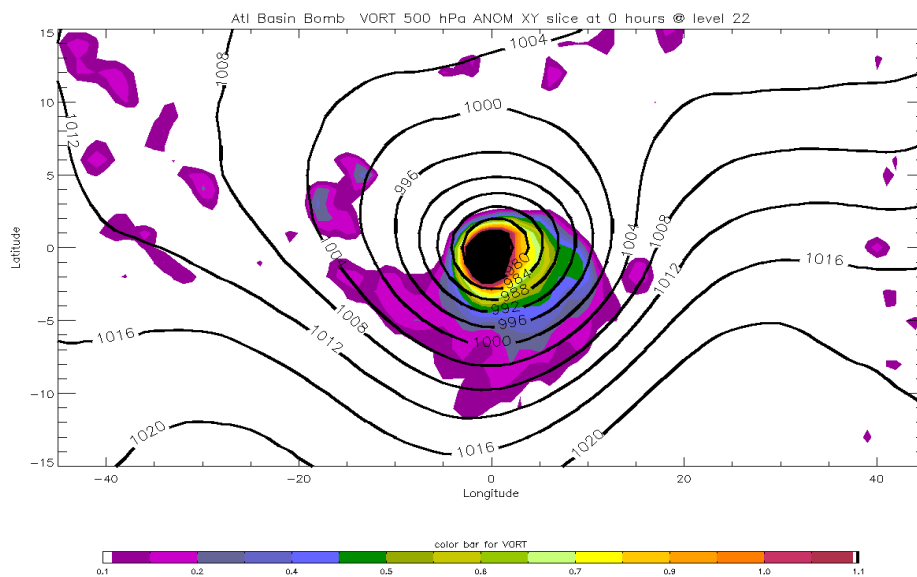
Figure 48.   Vorticity at 500 hPa anomaly composite at 0-hour of Atlantic basin
Black lines are SLP contours (intervals of 4 hPa).
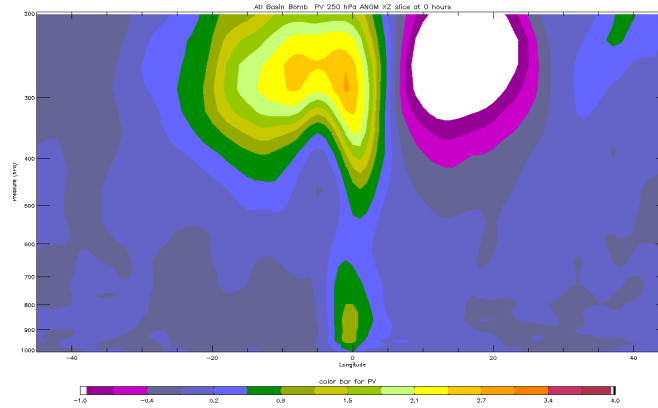
Figure 49.   0-hour vertical cross section anomaly composite of Atlantic basin
potential vorticity (PV). From 1000 hPa to 200 hPa.
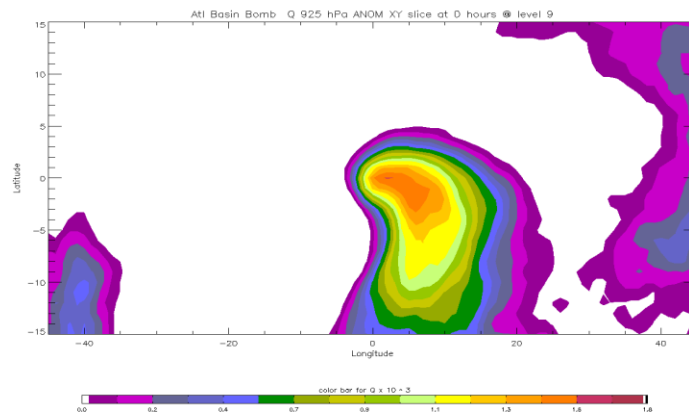
Figure 50.   Specific humidity anomaly composite at 0-hour for the Atlantic basin
at 925 hPa
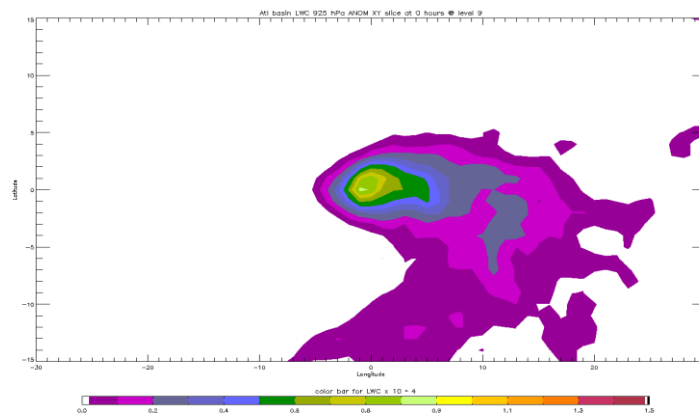
Figure 51.   Liquid water content anomaly composite at 0-hour of Atlantic at 925
hPa.
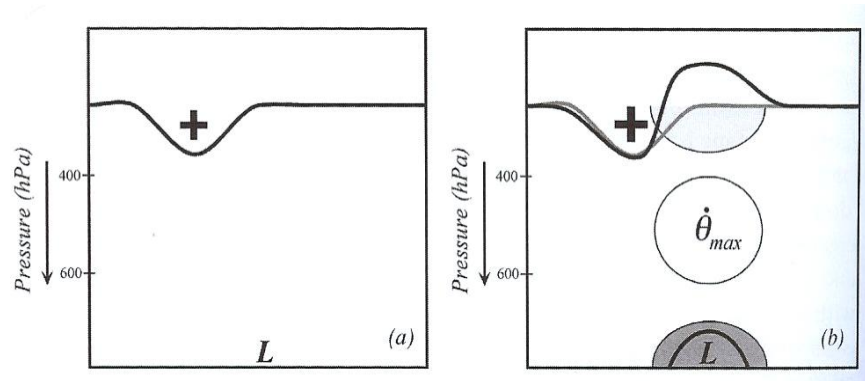
Figure 52. (a) Relationship between upper tropospheric positive PV anomaly and a surface low pressure center. (b) ascent downstream of the PV anomaly produces latent heat release manifest as a θ_{max}. PV erosion aloft deforms the bold PV contour to the east of the original anomaly making the anomaly even more anomalous (larger + sign). PV production in the lower troposphere intensifies the surface cyclone with the values of PV developing near the center indicated by the bold black line surrounding the 'L". (Adapted from Martin (2006)).

C.   EXPLOSIVE STAGE COMPOSITE

The explosive stage in our study refers to the 24-hour period when the extratropical cyclones experienced the most rapid deepening rate. During this 24-hour period, 75% of the hurricane force extratropical cyclones deepened explosively according to the > 1 hPa h^{-1} for 24-hours (geostrophically adjusted) criteria. The structure of the anomaly composites during this period are characterized by environmental conditions that are conducive to significant cyclogenesis events.

Examining the evolution of the 500 hPa vorticity anomaly composites from 24 hours to 6 hours prior to the 0-hour anomaly composite shows a classic signature of a growing or intensifying cyclogenesis event. Figure 53a displays the upper lever trough displaced to the west, placing the area of divergence aloft above the surface low. This displacement allows for maximum evacuation of mass, which causes the surface low to rapidly deepen. By 6 hours prior to the 0-hour, the positive vorticity anomaly has moved closer to the position of the surface low (Figure 53d).

We have discussed how moisture can contribute to the intensification of an extratropical cyclone. A plot of the specific humidity available 24 and 6 hours prior to the 0-hour identifies anomalous values of moist, likely due to the flow associated with the warm conveyor belt (Figure 54). The injection of moist air into the weather system likely facilitated the intensification of the system.

The anomaly composite of the total wind at 250 hPa 24 hours prior to the 0-hour composite captures a jet streak (Figure 55a). When compared with the anomaly composite at the 0-hour (Figure 55b), the -24 hour plot shows a stronger wind velocity anomaly. A strong jet streak is conducive to cyclogenesis because the exit region of the jet is favorable for upper-level divergence and rising motion throughout the column.

A west-east vertical cross section of the composite PV anomaly 24 hours prior to the 0-hour is presented in Figure 56. It depicts a large positive PV anomaly at the tropopause. As discussed earlier, positive PV anomaly is associated with cyclonic flow that may extend to the surface. The presence of such an anomaly can aid a cyclogenesis event.

Finally, the 925 hPa temperature anomaly composites are presented in Figure 57. The northwest to southeast negative-positive temperature anomaly couplet at -24 hours represent the enhanced baroclinicity associated with the events. Going forward in time, the cumulative effect of the cold and warm low-level advection associated with the cyclone becomes more evident.

Figure 53. Vorticity anomaly composite of Atlantic at 500 hPa. Black lines are SLP (interval of 4 hPa). (a) 24-hours prior to 0-hour composite. (b) 18-hours prior to 0-hour composite. (c) 12-hours prior to 0-hour composite. (d) 6-hours prior to 0-hour composite.
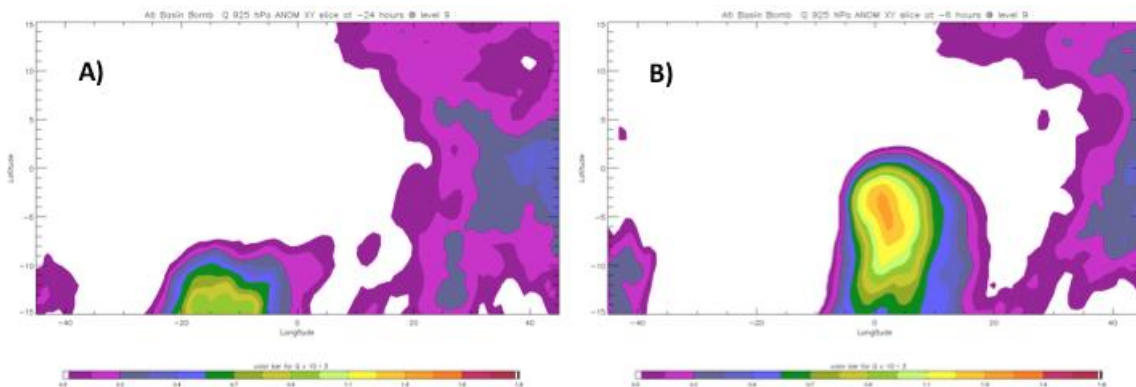
Figure 54. Specific humidity anomaly composite at 925 hPa. (a) 24-hours prior to the 0-hour composite. (b) 0-hour anomaly composite
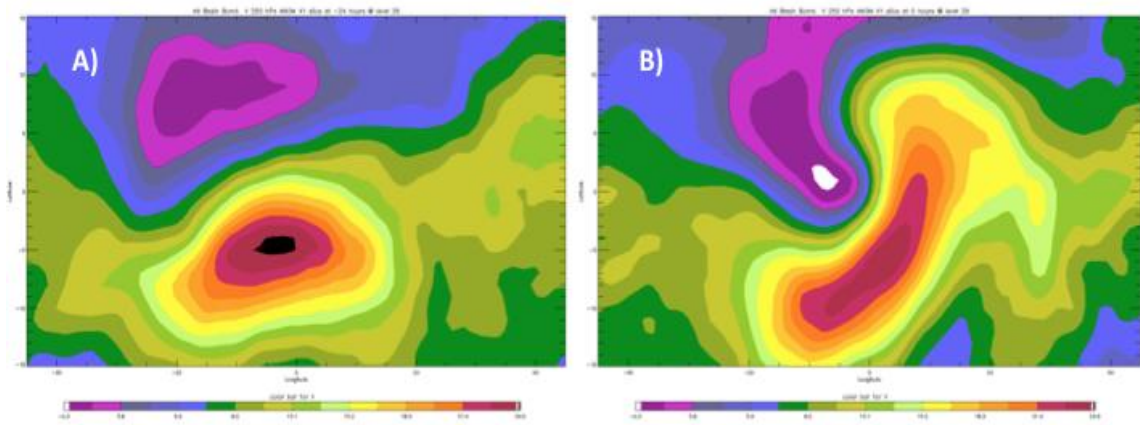
Figure 55. Velocity anomaly composite plot of the Atlantic at 250-hPa. Colors represent wind velocity from -0.3 ms^{-1} to 24.5ms^{-1}. (a) 24-hour prior to 0-hour. (b) 0-hour anomaly composite
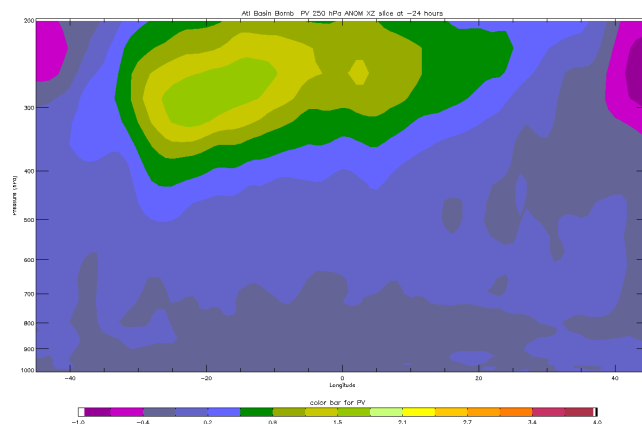
Figure 56. Vertical cross section PV anomaly composite of the Atlantic basin. Cross section is from 1000 hPa to 200 hPa. Contours rage from -1.0 to 4. Light green contour is 2.0 PVU
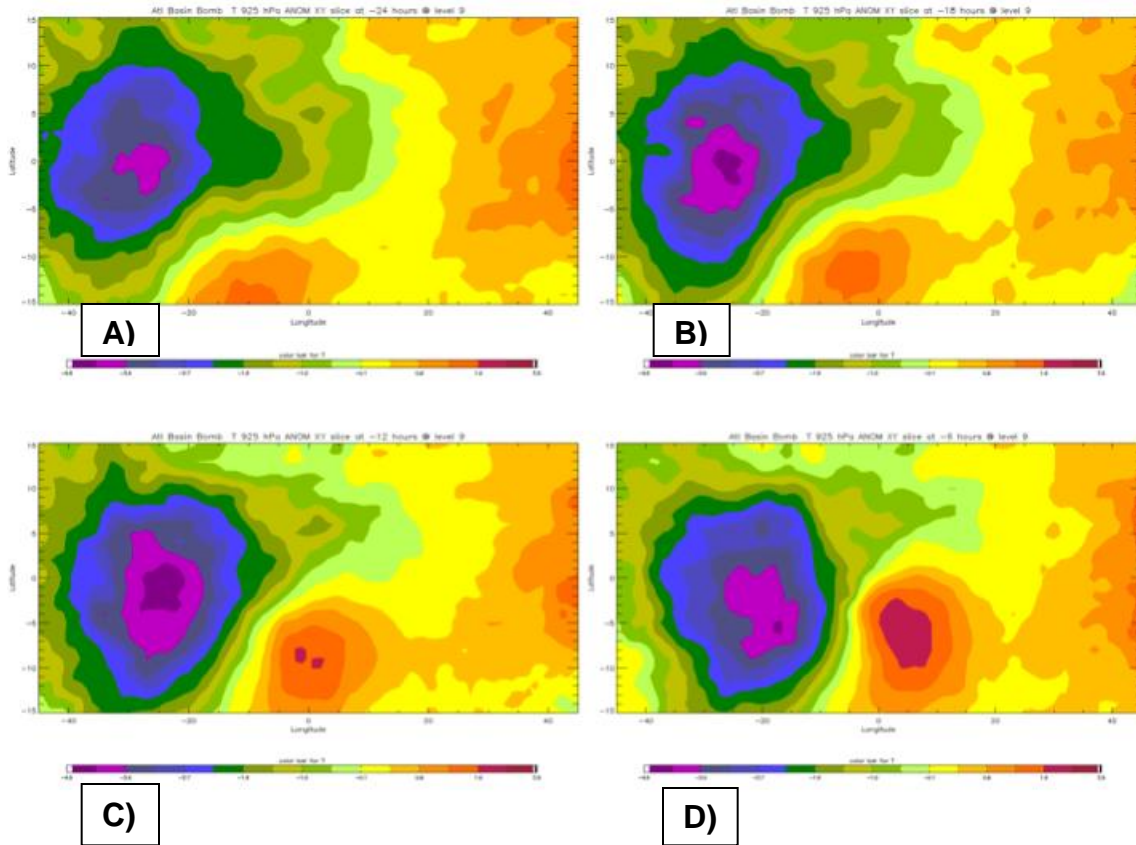
Figure 57. Temperature anomaly composite at 925 hPa of the Atlantic basin. Temperature ranges from -4.5 to 2.5 degrees Celsius. (a) 24 hours prior to 0-hour. (b) 18 hours prior to 0-hour. (c) 12 hours prior to 0-hour. (d) 6 hours prior to 0-hour.

D. DECAY STAGE COMPOSITES

The decay stage of extratropical cyclones occurs when the upper level divergence maximum becomes displaced to the east of the SLP minimum (Martin 2006). The surface pressure begins to rise because there is no longer a mechanism removing mass aloft. Consequently, as the pressure rises cyclonic flow decreases and there is a reduction in surface geostrophic vorticity (Martin 2006). One can consider the decay stage as a reverse of the cyclogenesis process. The same sort of positive feedback-loop that serves to rapidly intensify a hurricane force extratropical cyclone, is responsible for the rapid decay of a cyclone, or cyclolysis of a storm. Since the divergence maximum is displaced to

61

the east and there is no more upward vertical motion over the center of the storm system, the upper level trough begins to flatten and the radius of curvature of the upper level trough increases (Martin 2006). The radius increase reduces positive vorticity advection, further reducing upward vertical motion. As a result, the surface pressure rises rapidly, which further exacerbates the situation.

The vertical stacking of the upper level trough and the low-pressure center at the surface marks the end of the growth stage of a cyclone. By the end of the explosive stage, the composites showed a nearly vertically stacked system. The hurricane force extratropical cyclones continue to experience deepening for an average of 6 hours after the maximum deepening rate. It is at this point that the decay stage begins. Our composites are consistent with this theory of cyclolysis.

Examining the vorticity anomaly at 500 hPa composite at 24 and 48 hours after the 0-hour yield results consistent with previous studies on cyclolysis. Figure 58a–b show the results. The positive vorticity at the upper level is all but gone. And the surface pressure gradients have weakened.

The 925 hPa temperature anomaly composite 24 and 48 hours after the 0-hour are presented in Figure 59a–b. The cold and warm temperature anomaly couples is shown to weaken with time. Also, the temperature advection pattern due to the cyclone can be discerned. Heat has been transported poleward and cooler temperatures have been moved equatorward.

Finally, the upper level support from the jet streak noted earlier in the lifecycle of the extratropical cyclone is all but gone by the 48th hour after the 0-hour composites. Figure 60a–b display 250 hPa total wind anomalies. By the 24th hour after the 0-hour composite, a weaker jet streak is observed but the position relative to the surface low has changed. By the 48th hour, the wind velocity anomaly is weaker and farther east.
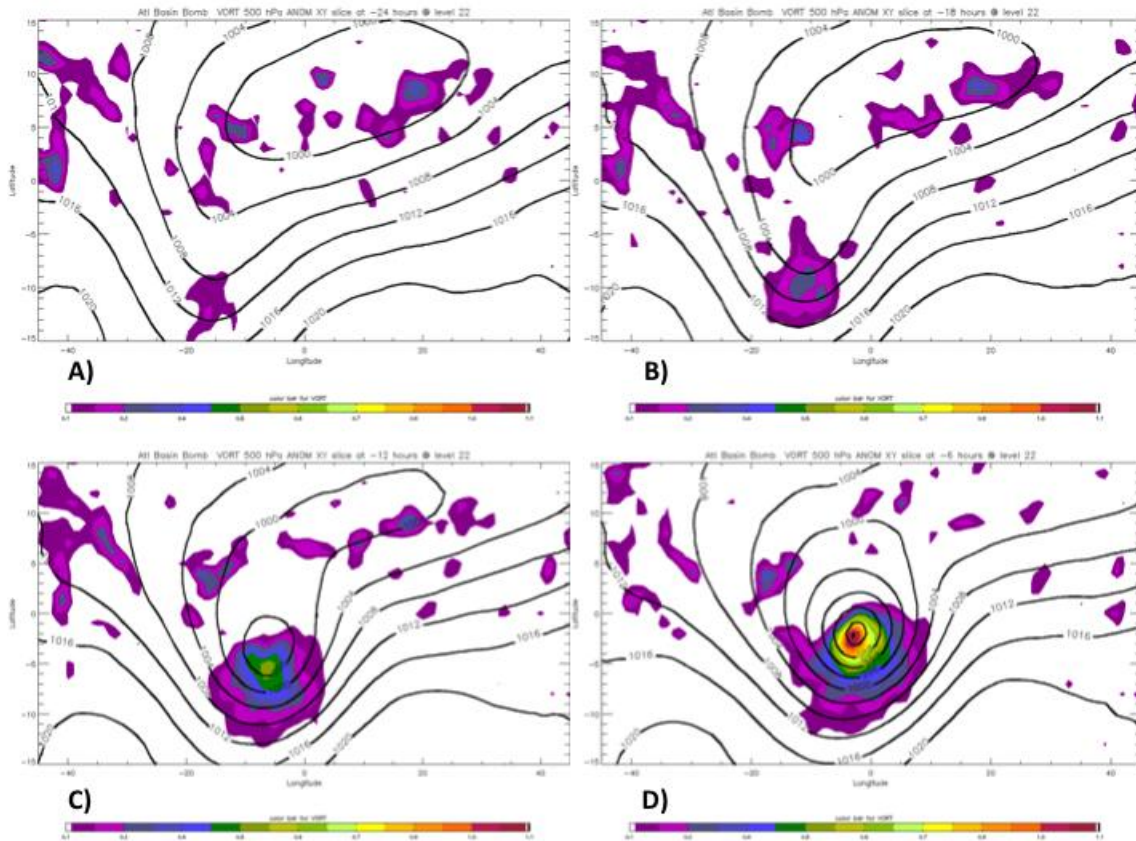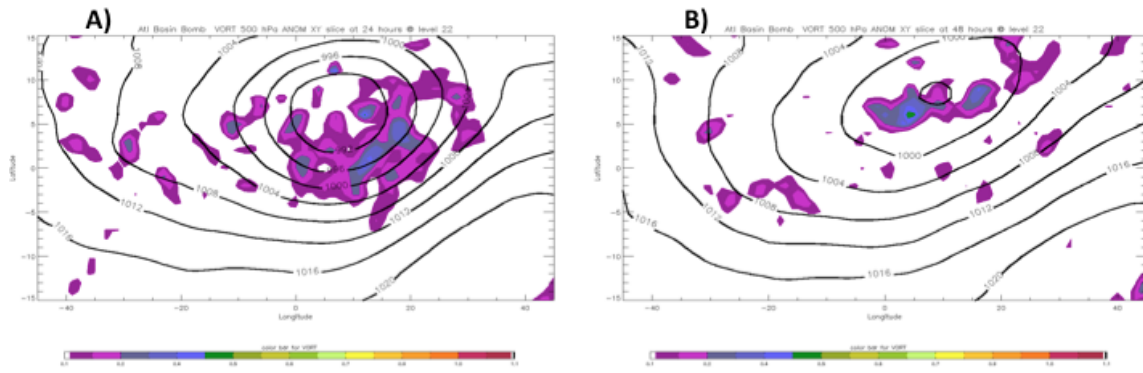
Figure 58.　Vorticity anomaly composite of Atlantic at 500 hPa Black lines are SLP (interval of 4 hPa). (a) 24-hours after 0-hour. (b) 48-hours after 0-hour.

Figure 59.　Temperature anomaly composite of Atlantic at 925 hPa. Temperature range from -5 to 2 degrees Celsius. (a) 24-hours after 0-hour. (b) 48-hours after 0-hour
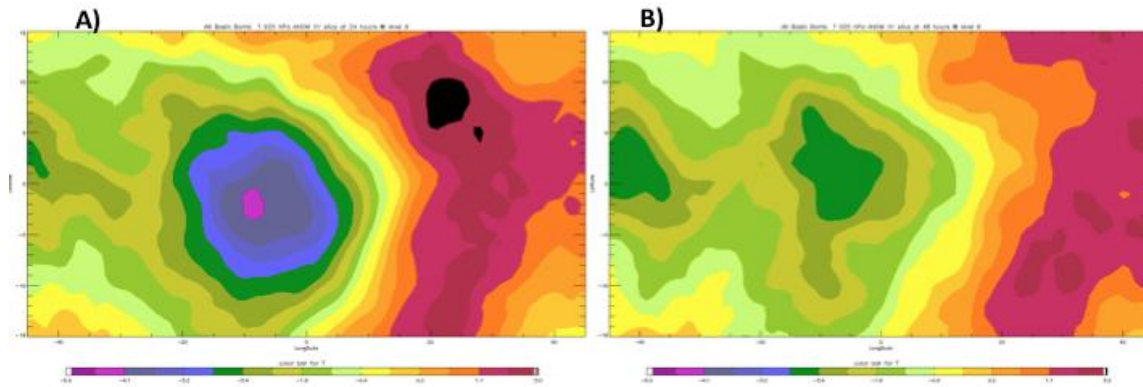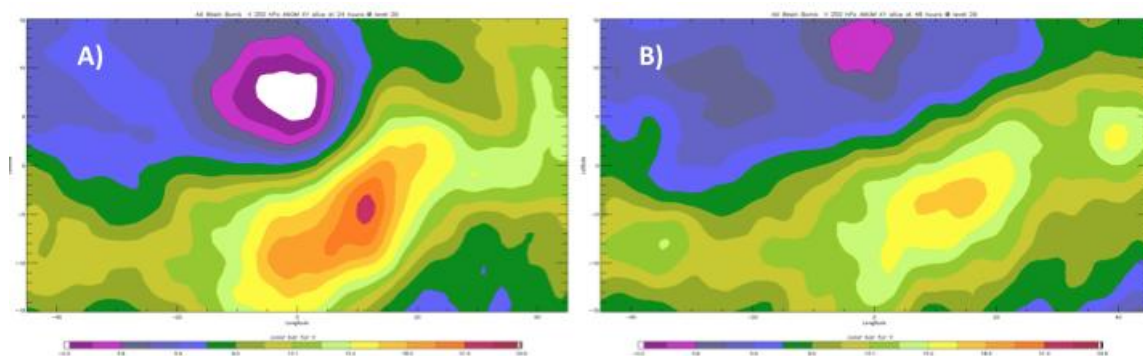

Figure 60.　Velocity anomaly composite of the Atlantic at 250-hPa. Velocity range from -0.3 ms^{-1} to 24.5ms^{-1}. (a) 24-hours after 0-hour. (b) 48-hours after 0-hour

THIS PAGE INTENTIONALLY LEFT BLANK

V.   PREDICTABILITY ANALYSIS

The goal of this section is to take a first look at the probabilistic prediction of hurricane-force extratropical cyclones. Two Atlantic storms were chosen at random. Ensemble prediction data from the ECMWF and NCEP were obtained from the TIGGE database. A sea level pressure (SLP) tracking algorithm was created to identify and track the storm center in each ensemble member. The track and SLP evolution were catalogued, allowing for the comparison of each ensemble member with the ensemble mean and the observed evolution in the NWS OPC database.

A.   NOVEMBER 2007 STORM

The first storm selected randomly for the qualitative analysis of the ECMWF and NCEP ensemble model prediction system occurred in the Atlantic basin in the month of November during the 2007–2008 cold season.

To examine the 'best guess' evolution of the first randomly selected storm, dynamic tropopause (DT) maps with SLP overlays were constructed using ERA-interim data and are presented in Figure 61a–g. The wave-guide (and jet stream) is located in these maps where there is a large potential temperature gradient over a short horizontal distance.

In Figure 61a, a nascent SLP minimum is located over Nova Scotia to the east of a distinct tropopause-level positive PV anomaly (seen as a negative potential temperature anomaly on the DT maps). The westward tilt with height between the surface low center and the upper-level positive PV anomaly is conducive for the intensification of the system as a whole. Consistent with this notion, the surface low is observed to deepen and the wavelike feature along the DT shortens its wavelength.

With time, the westward tilt with height is observed to lessen, becoming vertically stacked at 12 UTC 29 November (Figure 61e). It is at this time that the storm completes its 24-hour period of maximum rapid deepening (1.32 Bergeron)

and it first attains hurricane force winds. In terms of SLP, the storm moderately deepens over the subsequent six hours and then begins to fill. Yet, it did retain hurricane force winds for an additional 30 hours (until 18 UTC 30 November). The storm evolution depicted here is very similar to that of the composite analyses.

Following the minimum SLP center of the November 2007 extratropical cyclone in Figures 61 would yield a storm track that originates over Nova Scotia, migrates east, passes south of Greenland and terminates just west of Iceland. Some of the ensemble member in the ECMWF and NCEP prediction systems did a good job of prediction the storm track and intensity while others performed more poorly. Figures 62 and 63 show examples of a good and bad predicted track from ECMWF ensemble members. The asterisk marks the SLP minimum, and the colors depict the SLP ranging from 950 hPa to 1050 hPa. Figure 62 shows ECMWF ensemble member 8 predicting a track reasonably close to that observed. Figure 63 shows a poor track from ECMWF ensemble member 7.
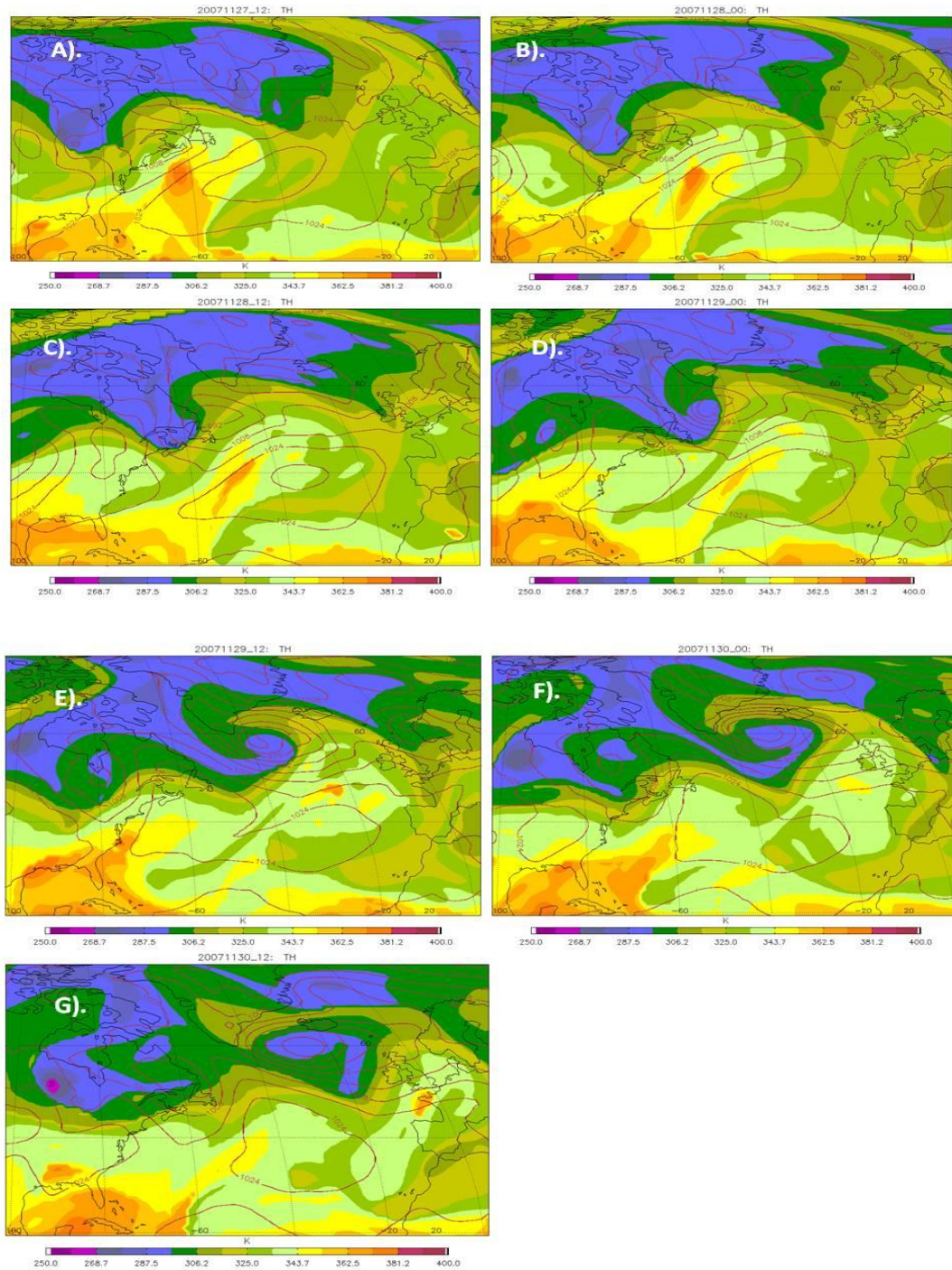
Figure 61. 12-hour interval dynamic tropopause chart and SLP chart of November 2007 hurricane force extratropical cyclone. Color contours are potential temperature (θ) and red lines are SLP in 8 hPa intervals. A). Nov 27 1200 UTC; B). Nov 28 0000 UTC; C). Nov 28 12000 UTC; D). Nov 29 0000 UTC; E) Nov 29 1200 UTC; F) Nov 30 0000 UTC; G) Nov 30 1200 UTC
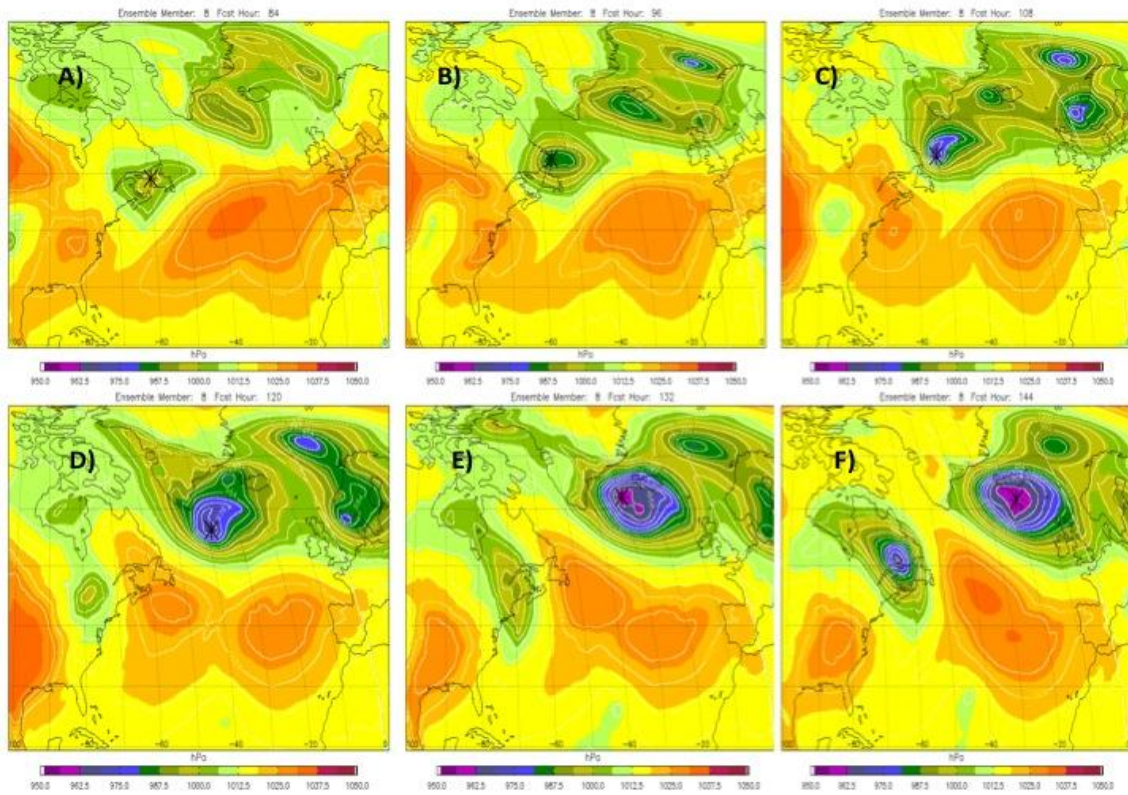
Figure 62.   ECMWF ensemble member 8, track and SLP minimum intensity prediction. Black asterisk marks the SLP minimum. White lines are isobars in 4 hPa intervals. Colors are SLP ranging from 950 hPa to 1050 hPa. A) 84-hour of 144-hour forecast; B) 96-hour of 144-hour forecast; C) 108-hour of 144-hour forecast; D) 120-hour of 144-hour forecast; E) 84-hour of 132-hour forecast; F) 144-hour of 144-hour forecast
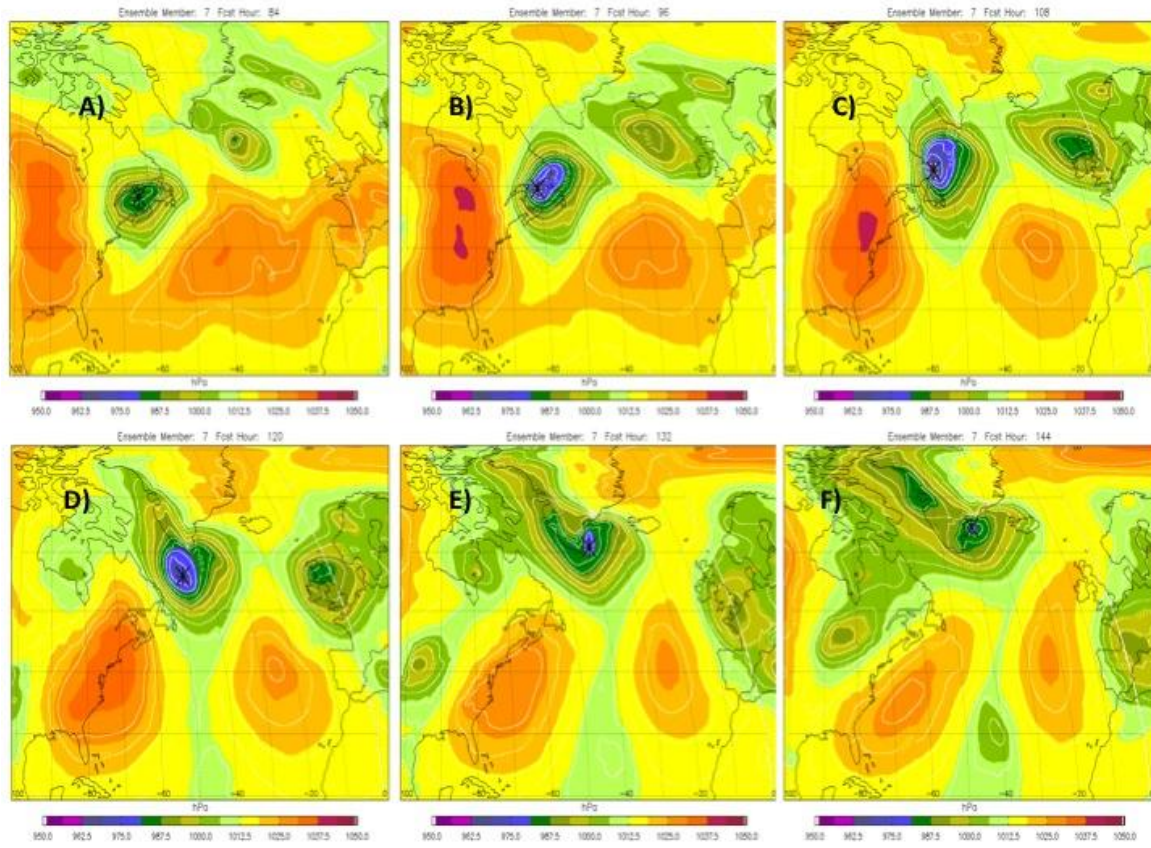
Figure 63.   ECMWF ensemble member 7, track and SLP minimum intensity prediction. Black asterisk marks the SLP minimum. White lines are isobars in 4 hPa intervals. Colors are SLP ranging from 950 hPa to 1050 hPa. A) 84-hour of 144-hour forecast; B) 96-hour of 144-hour forecast; C) 108-hour of 144-hour forecast; D) 120-hour of 144-hour forecast; E) 84-hour of 132-hour forecast; F) 144-hour of 144-hour forecast

Summary plots of the minimum SLP track and SLP intensity versus time of the ECMWF and NCEP ensemble members allow for a comparison with the ensemble mean and observed data. Figures 64 and 66 show the spread of the positions forecasted by the 51 ensemble members of the ECMWF model and the 21 ensemble members of the NCEP model. The purple track is the ensemble mean while the red track is the observed track. Comparing the ensemble mean to the observed track shows that both ensemble prediction systems did a good job forecasting the track of the cyclone.

The ECMWF shows a slight bias to the north, the mean predicts a more northerly storm track, while the ensemble mean of the NCEP shows a slight bias to the south.

.
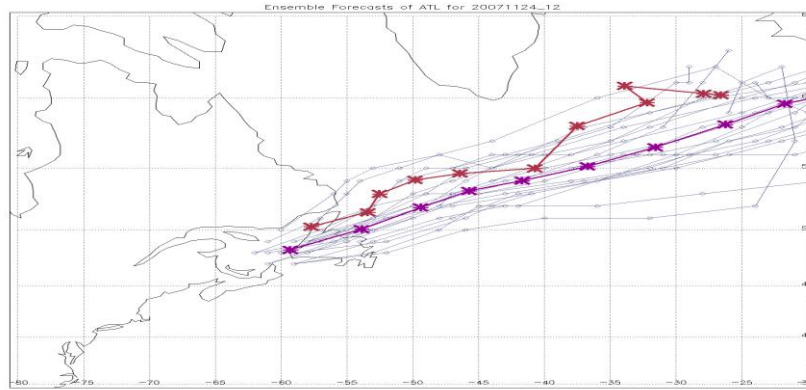
Figure 64.   NCEP ensemble prediction tracks for 21 ensemble members. Red track is the observed track of cyclone. Purple track is the ensemble mean. Stars along the tracks denote 6-hour time steps starting from 28 November at 0000Z.

Figure 65.   NCEP ensemble prediction plot of November 2007 extratropical cyclone SLP intensification. Red line is the observed data, purple is the ensemble mean. Stars along the plots denote 6-hour time-steps starting from 28 November at 0000Z.

Figure 66.   ECMWF ensemble prediction tracks for 21 ensemble members.
Red track is the observed track of cyclone. Purple track is the
ensemble mean. Stars along the tracks denote 6-hour time steps
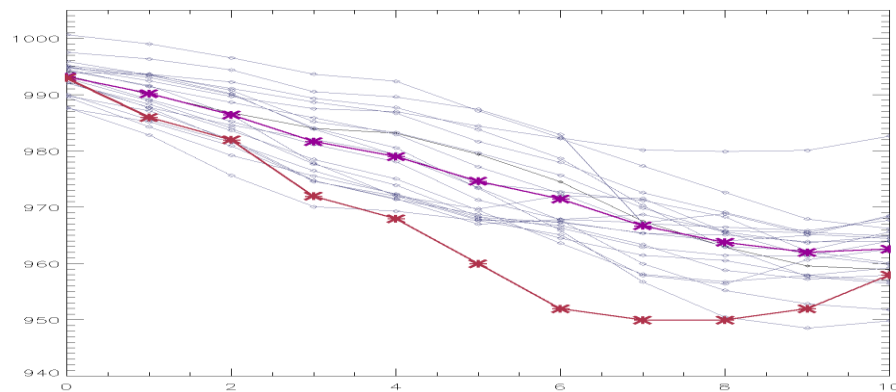starting from 28 November at 0000Z.

Figure 67.   ECMWF ensemble prediction plot of SLP intensification. Red line is
the observed data, purple is the ensemble mean. Stars along the
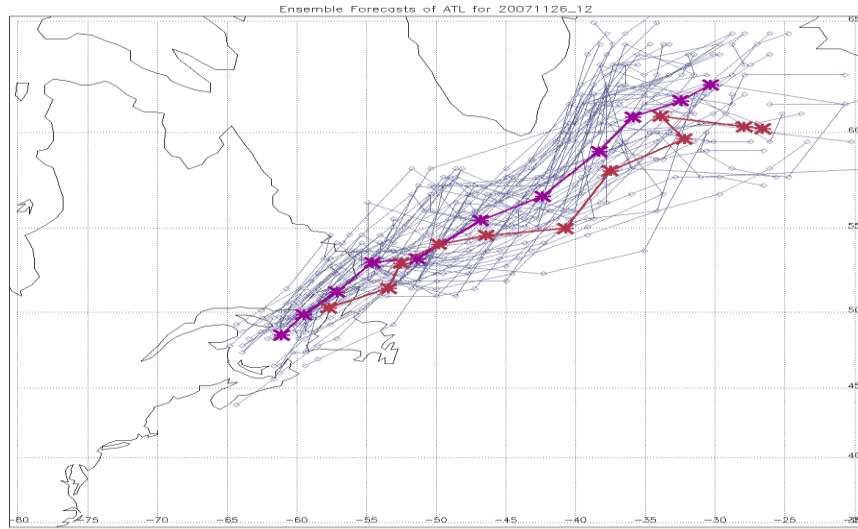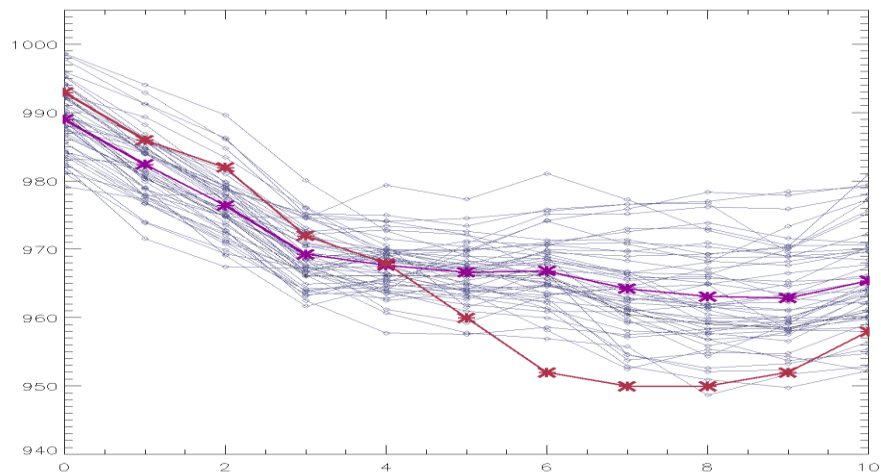plots denote 6-hour time steps starting from 28 November at 0000Z.

71

The SLP intensification plots in Figures 65 and 67 show the ensemble prediction systems did a relatively poor job predicting the deepening of the storm system. The x-axis of the plot is numbered 0–10. The numbering corresponds to 6-hour incremental time-steps. The 24 hour of explosive deepening the extratropical cyclone experienced occurred between time step 2 and 6 (24 hours). The ECMWF ensemble members predicted the first 12 hours of deepening relatively well but did poorly over the last 12 hours of explosive deepening. The NCEP ensemble mean showed the model doing a poor job predicting the SLP intensification during the whole 24-hour period of explosive deepening.

One might reasonably argue that the results are skewed due to the coarse resolution of the ensemble data. As will be seen in the next example, this does not appear to be the case.

B. JANUARY 2008 STORM

The second randomly selected storm occurred in January during the 2007–2008 cold season. The storm evolution plotted from the observed data from ECMWF shows an evolution similar to the November 2007 storm despite the difference in intensity. The January 2008 storm attained a 2.09 Bergeron after 24-hours of explosive deepening. Only 14.5% of all hurricane force extratropical cyclones in the Atlantic and Pacific basins exhibited 2.0 or greater Bergeron.

Similar to the November 2007, the SLP minimum is displaced to the east of the upper level positive anomaly in Figure 68a. As the storm intensifies the SLP minimum and upper level anomaly become vertically stacked. Figure 68c, which is 21 January 1200 UTC, corresponds to the time when the storm first exhibits hurricane force winds and it is also when the extratropical cyclone completed 24 hours of explosive deepening. At this time, the plot shows that the SLP minimum is not vertically stacked, in comparison to the November 2007

storm at the same stage. Hurricane force winds of the January 2008 storm persisted for approximately 12-hours longer than in the November 2007 storm.
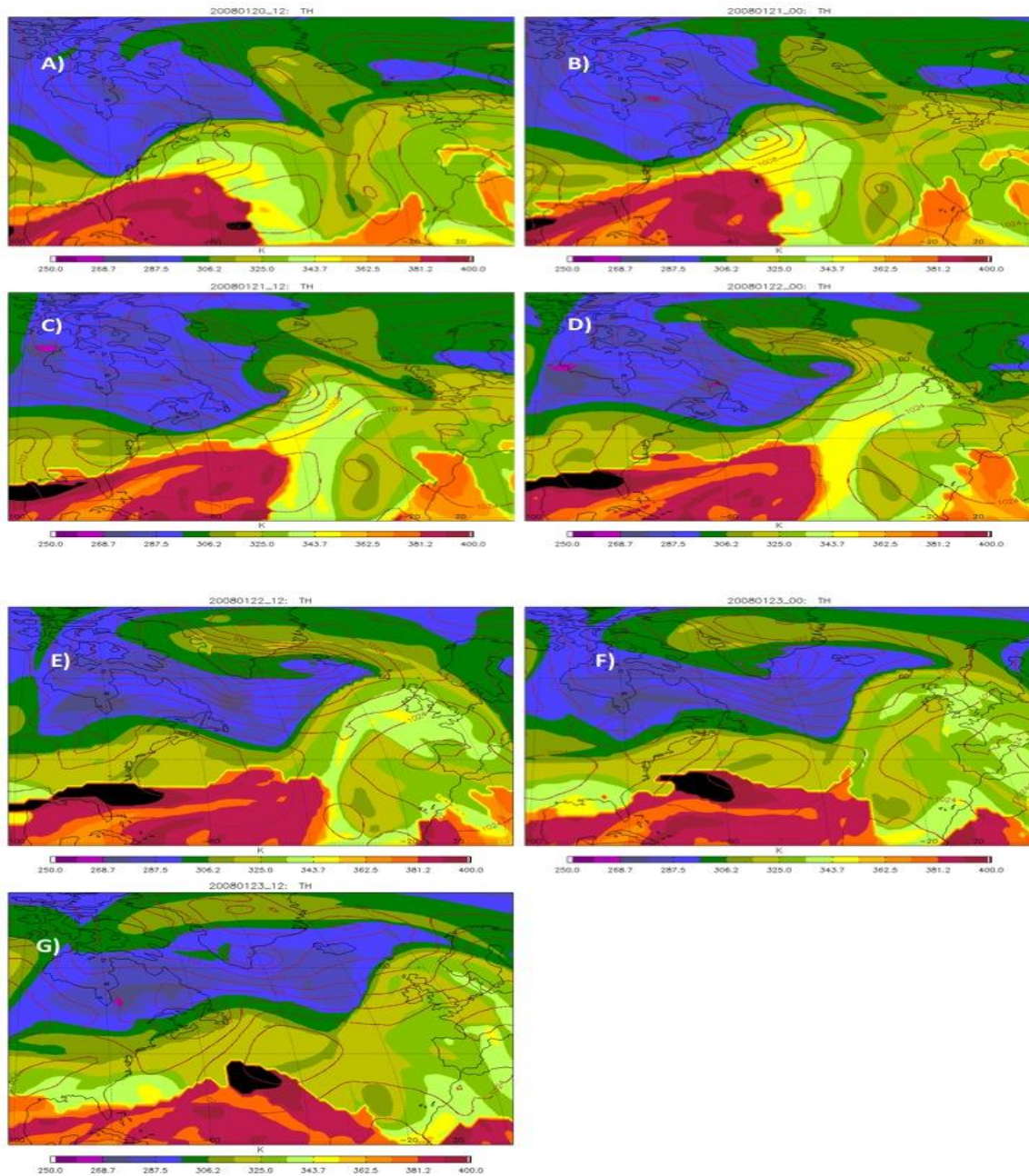

Figure 68.   12-hour interval dynamic tropopause chart and SLP chart of January 2008 hurricane force extratropical cyclone. Color contours are potential temperature (θ) and red lines are SLP in 8 hPa intervals. A) Jan 20 1200 UTC; B) Jan 21 0000 UTC; C) Jan 21 1200 UTC; D) Jan 22 0000 UTC; E) Jan 22 1200 UTC; F) Jan 23 0000 UTC; G) Jan 23 1200 UTC

The ECMWF and NCEP ensemble model prediction systems used for the summary plots were initialized on the January 16 at 1200 UTC. The 108-hour forecast of a 144-hour forecast corresponds to January 21 at 0000 UTC time-step, the first time step plotted for qualitative model performance evaluation.

Six time-steps starting from January 21 at 0000Z, on to the 22nd at 1200Z are plotted on the ensemble mean and observed tracks. The same six time steps are plotted on the SLP intensification plot.

On the x-axis of the SLP intensification and the ensemble prediction tracks, time-step 2 corresponds to the end of the explosive deepening period. Figures 70 and 72 show that the prediction of the SLP evolution is significantly better than for the November 2007 case. A larger number of ensemble members predict a SLP intensification that closely matches the observed data.

In contrast, Figures 69 and 71 show the models having some difficulty with predicting the storm track. The ensemble mean of both models do not come close to the observed track of the storm. The ECMWF ensemble mean once again shows a track that is to the north of the observed track. The NCEP ensemble mean exhibits a track that initially starts right on top of the observed track, but diverges quickly to the north of the observed track.

Both ensemble prediction systems were 144-hour forecasts (6 days) which would contribute to some inaccuracy, but what the two randomly selected storms show is that the models have some difficulty predicting the highly dynamic evolution of events like hurricane force extratropical cyclones

Figure 69.   January 2008 extratropical cyclone. ECMWF ensemble prediction
tracks for 51 ensemble members. Red track is the observed track of
cyclone. Purple track is the ensemble mean. Stars along the tracks
denote 6 hour time steps starting from 21 January at 0000Z.

Figure 70.   ECMWF ensemble prediction plot of Jan 2008 extratropical cyclone
SLP intensification. Red line is the observed data, purple is the
ensemble mean. Stars along the plots denote 6 hour time steps
starting from 21 January at 0000Z.

Figure 71.   January 2008 extratropical cyclone. NCEP ensemble prediction
tracks for 51 ensemble members. Red track is the observed track of
cyclone. Purple track is the ensemble mean. Stars along the tracks
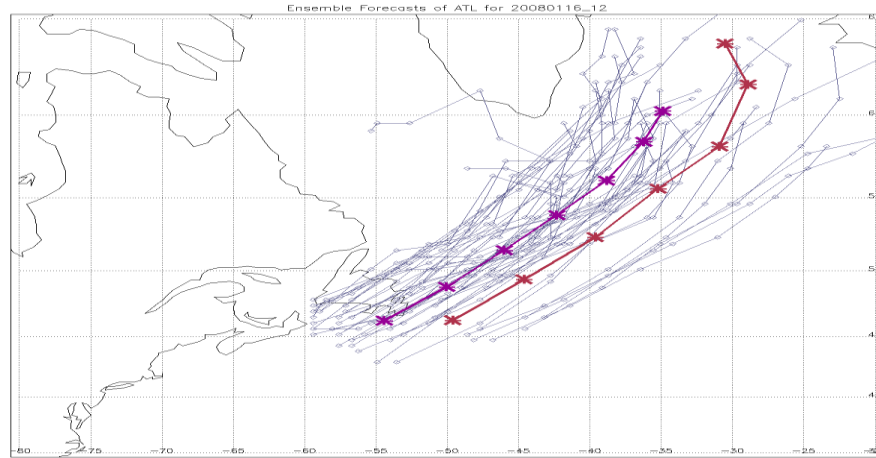denote 6 hour time steps starting from 21 January at 0000Z

Figure 72.   January 2008 extratropical cyclone. NCEP ensemble prediction
tracks for 51 ensemble members. Red track is the observed track of
cyclone. Purple track is the ensemble mean. Stars along the tracks
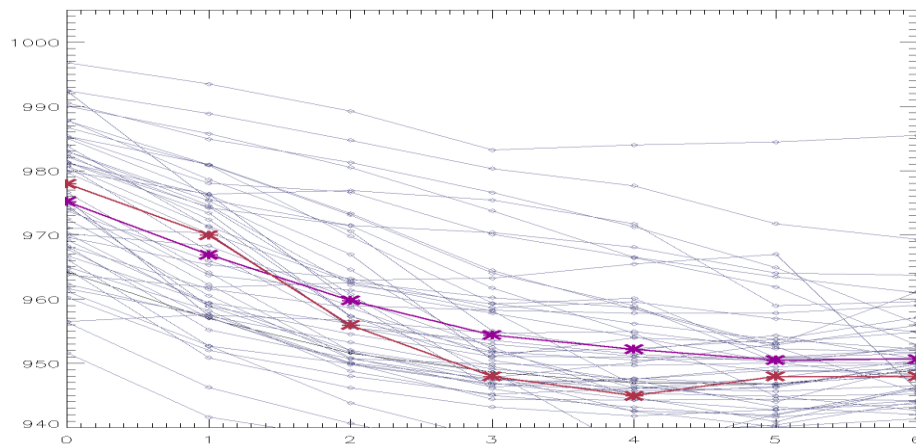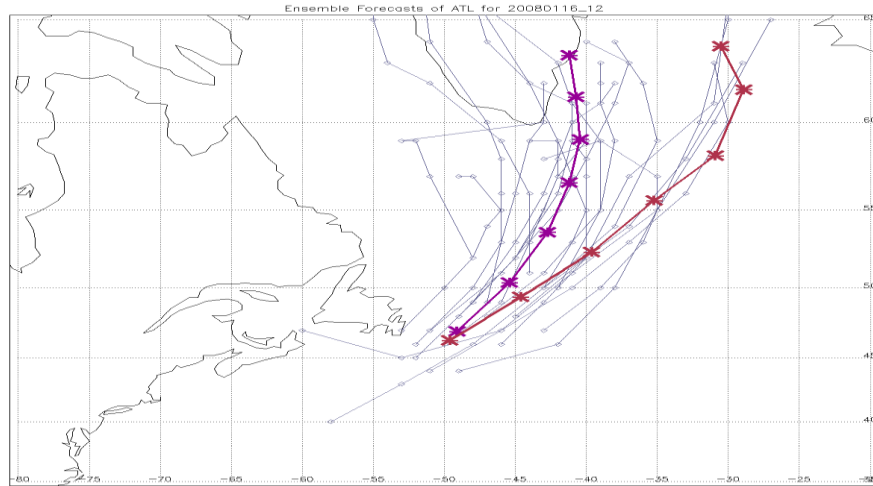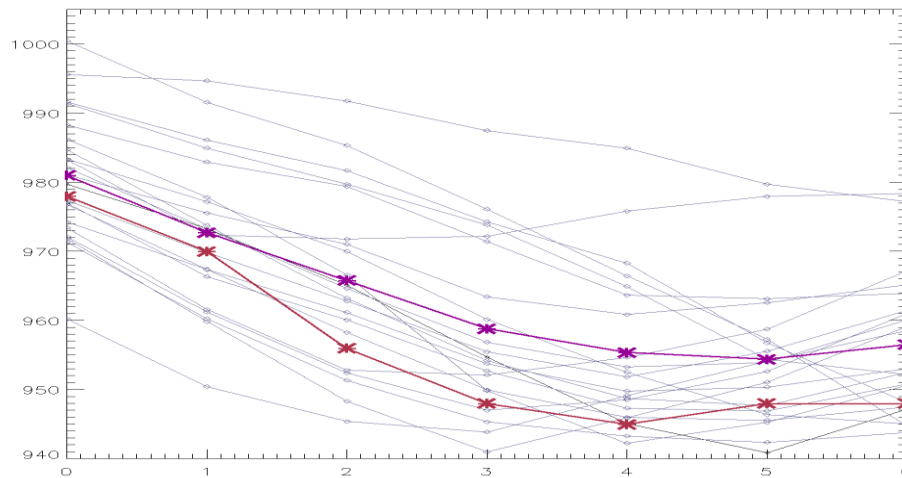denote 6-hour time steps starting from 21 January at 0000Z.

VI. SUMMARY, CONCLUSIONS AND FUTURE RESEARCH

A. SUMMARY AND CONCLUSIONS

Using data compiled by the National Weather Service Ocean Prediction Center, a hurricane force extratropical cyclone climatology for three colds seasons was created. A total of 259 storms, nearly evenly split between the Atlantic and Pacific basins, were catalogued. It is found that 75% of these storms met the criteria for a bomb [as defined by Sanders and Gyakum (1980)].

Comparisons of these data with previous climatological studies of extratropical cyclones showed a good overall agreement despite the use of a number of different datasets and methodologies. The frequency maximum of hurricane force extratropical cyclones in the Atlantic basin is located the southeast of Greenland. In the Pacific, two maxima to the east of Japan were identified. These regions agree well with previous results for extratropical cyclones of all intensities. This beckons the question whether hurricane force extratropical cyclones are dynamically different or just more intense variants of a typical extratropical cyclone.

Composite analyses illustrated that these storms formed in regions with anomalously strong baroclinicity, as might be expected. The surface low formed and began to intensify upstream of an upper-level positive PV anomaly. This westward tilt with height is conducive to the amplification of the system as a whole. Over time, the westward tilt with height was observed to lessen. By the end of the 24-hour period of maximum deepening rate, the storm system was observed to be nearly vertically stacked. On average, the storms continued to deepen (in terms of minimum SLP) for an additional six hours, thereafter beginning to fill. In addition to the obvious baroclinic processes at work, there is some indication that diabatic heating served as an additional energy source for the storms in question. All of these findings are, once again, consistent with the known structure and evolution of extratropical cyclones.

77

To briefly examine the predictability of these systems, two storms were randomly selected for further study. Ensemble prediction data from the ECMWF and NCEP were acquired. The results indicated that, while both systems did an admirable job of representing the event, features of the storm were not captured within the model spread. In the case of the November 2007 storm, no member properly simulated the deepening rate and ultimate intensity of the observed storm. In contrast, for the January 2008 case, both ensemble prediction systems had a difficult time simulating the track of the storm.

B.   FUTURE RESEARCH

There are three clear avenues for further research on this topic. The composite analyses clearly identified distinct anomalies associated with these events. It is imperative to determine if these anomalies are in fact statistically significant. This can be quantified by using a Monte Carlo approach to test the randomness of the identified anomalies.

Herein, we took a brief first look at the predictability of these events by ensemble prediction systems. It would be useful to greatly expand the work on this issue but examining both more storms and different ensemble prediction systems.

Finally, numerical simulations of a number of cases would prove quite insightful in terms of the dynamical evolution of these systems. It would specifically help address the question regarding the importance of diabatic processes.

LIST OF REFERENCES

Bosart, L.F., 1981: The Presidents' Day Snow Storm of 18–19 Febuary 1979: A synopitc scale event. *Mon. Wea. Rev.,* **109**, 1542–1566.

Browning, K.A., 2003: The sting at the end of the tail: Damaging winds associated with extratropical cyclones. *Q.J.R Meteorl. Soc*, **130**, 375–399.

Carlson, T.N., 1980: Airflow through midlatitude cyclones and the comma cloud pattern. *Mon. Wea. Rev.*, **108**, 1498–1509.

Danielson, E.W., J. Levin, E. Abrams, 2002: *Meteorology.* 2nd ed. McGraw-Hill Higher Education, 576 pp.

Dee, D.P., and Coauthors, 2011: The ERA-Interim reanalysis: configuration and performance of the data assimilation system. *Q.J.R Meteorl. Soc*, **137**, 553–597.

Gyakum, J.R.: On the Evolution of the *QE II* Storm. II: Dynamic and Thermodynamic Structure, *Mon, Wea. Rev.,* **111**, 1156–1173, 1983b.

Hoskins, B. and K.I. Hodges, 2002: New Perspective on the Northern Hemisphere Winter Storm Tracks. *J.A.S.*, **59**, 1041–1061.

Martin, J. E., 2006: *Mid-Latitude Atmospheric Dynamics*. John Wiley and Sons, 324 pp.

Reed, R.J, and Coauthors, 1988: The Role of Latent Heat Release in Explosive Cyclogenesis: Three Examples Based on ECMWF Operational Forecasts. *J.A.S.,* **3**, 217–229.

Roebber, P.J., 1984: Statistical Analysis and Updated Climatology of Explosive

Cyclones. *Mon. Wea. Rev.*, **112**, 1577–1589.

Rogers, E., and L.F. Bosart, 1986: An Investigation of Explosively Deepening Oceanic Cyclones. *Mon. Wea. Rev.*, **114,** 702–718.

Sanders, F., and J.R. Gyakum, 1980: Synoptic-Dynamic Climatology of the "Bomb". *Mon. Wea. Rev.*, **108**, 1589–1606.

Sienkiewicz, J. M., M. J. Brennan, and S. G. Winterberger, 2008: A Look at Hurricane Force Extratropical Cyclones. 14th Cyclone Workshop, Sainte Adele, Quebec, Canada.

Wernli, H., and C. Schwierz, 2006: Surface Cyclones in the ERA-40 Dataset (1958–2001). Part I: Novel Identification Method and Global Climatology. *J.A.S.,* **63**, 2486–2507.

INITIAL DISTRIBUTION LIST

1. Dudley Knox Library
   Naval Postgraduate School
   Monterey, California

2. Prof. Richard Moore
   Naval Postgraduate School
   Monterey, California

3. Prof. Wendell Nuss
   Naval Postgraduate School
   Monterey, California